Synthesis, Structural Characterization, and Electronic Properties of the Ph_4P^+ Salts of the Mixed Terminal Ligand Cubanes $Fe_4S_4(Et_2Dtc)_n(X)_{4-n}^{2-}$ (X = Cl^-, PhS^-) (n = 1, 2). Two Different Modes of Ligation on the $[Fe_4S_4]^{2+}$ Core

M. G. Kanatzidis,[†] D. Coucouvanis,*[†] A. Simopoulos,[‡] A. Kostikas,[‡] and V. Papaefthymiou[‡]

Contribution from the Department of Chemistry, University of Michigan, Ann Arbor, Michigan 48109, and Nuclear Research Center "Demokritos", Aghia Paraskevi, Attiki, Greece. *Received October 31, 1984*

Abstract: Mixed terminal ligand iron-sulfur clusters of the type $[Ph_4P]_2Fe_4S_4(X)_{4-n}(Et_2NCSS)_n$ (X = SPh, Cl, n = 2 and X = Cl, n = 1) have been synthesized in good yields by the reaction of $[Ph_4P]_2Fe_4S_4(L)_2(X)_2$ (L = SPh, Cl and X = Cl) with 2 equiv of $Et_2NCSSNa\cdot 3H_2O$ and $[Ph_4P]_2Fe_4S_4Cl_4$ with 1 equiv of $Et_2NCSSNa\cdot 3H_2O$, respectively. The synthesis and crystal structures of $[Ph_4P]_2Fe_4S_4(Cl)_2(Et_2NCSS)_2$ [X = SPh (I), Cl (II), and $[Ph_4P]_2Fe_4S_4Cl_3(Et_2NCSS)$ (III)] are described in detail. Complexes I and II crystallize in the monoclinic space group $C2/c$ with cell constants a = 17.486 (3) Å, b = 18.240 (3) Å, c = 24.198 (3) Å, and β = 109.73 (1)° and a = 20.409 (6) Å, b = 13.873 (3) Å, c = 25.739 (9) Å, and β = 118.94 (2)°, respectively. Complex III crystallizes in the monoclinic space group $P2_1/c$ with cell constants a = 15.836 (2) Å, b = 17.803 (2) Å, c = 22.496 (3) Å, and β = 101.44 (1)°. In the structures of I and II the non-hydrogen atoms were refined anisotropically and hydrogen atoms were included in the structure factor calculation but not refined. In the structure of III the carbon atoms were refined isotropically while all other non-hydrogen atoms were assigned anisotropic temperature factors. The hydrogen atoms were treated as in I and II. Refinement by full-matrix least squares of 661 parameters on 3226 data for I, 343 parameters on 1919 data for II, and 402 parameters on 5038 data for III gave final R values 0.079, 0.056, and 0.051, respectively. The anions in I and II are located on crystallographic 2-fold axes. The mean Fe-S* bond lengths in I, II, and III are 2.291, 2.307, and 2.317 Å, respectively. The Fe_4S_4 units in I-III contain two structurally distinct iron sites. One of the sites has tetrahedrally coordinated iron atoms with PhS^- and Cl^- terminal ligands. The second site is rather uncommon and shows the iron atoms coordinated by the Et_2NCSS ligands in a bidentate fashion. The Fe-Fe distances are longer for the iron atoms associated with the chelating Et_2NCSS^- ligands (3.053 (3) Å for I, 3.045 (4) Å for II, and 2.936 (2) Å for III). The Fe-SPh bond in I is 2.281 (4) Å. The Fe-Cl bonds in II and III are found at 2.249 (4) and 2.231 (2) Å, respectively. The Et_2NCSS^- ligand coordination in I and II is asymmetric with unequal Fe-S(Dt) distances of 2.552 (4) Å and 2.436 (4) and 2.578 (4) and 2.421 (4) Å, respectively. In contrast the corresponding distances in III are 2.478 (2) and 2.469 (2) Å. The electronic ^1H NMR and solution magnetic studies are reported. Zero-field Mössbauer spectra of I-III show two well-resolved quadrupole doublets. At 77 K, IS_1 = 0.47, ΔE_{Q1} = 1.06, IS_2 = 0.64, and ΔE_{Q2} = 1.84 mm/s for I, IS_1 = 0.53, ΔE_{Q1} = 1.06, IS_2 = 0.62, ΔE_{Q2} = 1.85 mm/s for II, and IS_1 = 0.51, ΔE_{Q1} = 1.07, IS_2 = 0.64, and ΔE_{Q2} = 2.13 mm/s for III. Cyclic voltammetric studies for I-III and double-potential step chronoamperometry for I are described.

Within the general class of Fe/S proteins that contain Fe_4S_4 centers,[1] there exist several members that display unusual electronic properties. These properties are manifested mainly in the ^{57}Fe Mössbauer and EPR spectra and are not found in any of the available analogue complexes.[2]

In the ferredoxin from *B. stearothermophilus* the ^{57}Fe Mössbauer spectrum of the $(Fe_4S_4)^{2+}$ center shows[3] a broadened, asymmetric, quadrupole doublet which can be attributed to the overlapping of at least two components and suggests that the iron atoms in this Fe/S center are not equivalent. The appearance of two resolved quadrupole doublets in the spectrum of the reduced form of the protein, $(Fe_4S_4)^+$, shows that the reduction is localized predominantly on one pair of iron atoms which become ferrous in character with the other pair remaining essentially unchanged.

Unusual Mössbauer spectra and an uncommon electronic spin ground state ($S > {}^3/_2$) have been detected also for the oxidized "P clusters" of nitrogenase. The latter show two resolved quadrupole doublets in the Mössbauer spectrum consistent with two distinct iron sites.[4] These unique spectral properties may arise because of significant differences in the ligation of the Fe_4S_4 cores. Such differences could include expansion to give coordination for the iron atom ligation or replacement of thiolate terminal ligands by other donor atoms within the protein "backbone".[5]

Recently, we reported[6] on the syntheses and structures of a series of "mixed" terminal ligand $(Fe_4S_4L_2L_2')^{2-}$ clusters (L = Cl^-, PhS^-; L' = PhS , PhO^-). The electronic ground states and Mössbauer spectra of these molecules were very similar to those of the identical ligand environment $(Fe_4S_4L_4)^{2-}$ clusters.[2] Furthermore, the Mössbauer hyperfine parameters of the individual iron atoms in the "mixed" ligand clusters were very similar and precluded resolution of the two iron sites (FeS_3L, FeS_3L) to, at least, visual recognition. The results of this study suggested that "mixed" terminal monodentate ligand coordination was insufficient to drastically affect the electronic spin ground state or the Mössbauer characteristics of the Fe_4S_4 cores.

The alternate suggestion[4] that expansion of the coordination sphere for one of the iron atoms in the Fe_4S_4 sites may give rise to the unusual Mössbauer spectra of the "P clusters" prompted us to undertake the synthesis of $(Fe_4S_4L_4)^{2-}$ clusters with "mixed" ligation modes on the Fe_4S_4 core.

In this paper we describe the synthesis, structural characterization, spectroscopic properties, and electrochemical properties of the $(Ph_4P)^+$ salts of the $[Fe_4S_4(SPh)_2(Et_2Dtc)_2]^{2-}$ (I), $[Fe_4S_4Cl_2(Et_2Dtc)_2]^{2-}$ (II), and $[Fe_4S_4Cl_3(Et_2Dtc)]^{2-}$ (III) anions which contain two different terminal ligands and show differences in ligation for the iron atoms in the Fe_4S_4 core. A preliminary

[†] University of Michigan.
[‡] Nuclear Research Center "Demokritos".

(1) (a) Lovenberg, W., Ed. "Iron-Sulfur Proteins"; Academic Press: New York, 1973; Vol. I, II; 1977; Vol. III. (b) Spiro, T. G., Ed. "Iron-Sulfur Proteins"; Wiley: New York, 1982.
(2) Holm, R. H. *Acc. Chem. Res.* **1977**, *10*, 427.
(3) (a) Mullinger, R. N.; Cammack, R.; Rao, K. K.; Hall, D. O.; Dickson, D. P. E.; Johnson, C. E.; Rush, J. D.; Simopoulos, A. *Biochem. J.* **1975**, *151*, 75. (b) Middleton, P.; Dickson, D. P. E.; Johnson, C. E.; Rush, J. D. *Eur. J. Biochem.* **1980**, *104*, 289.
(4) (a) Zimmerman, R.; Münck, E.; Brill, W. J.; Shah, V. K.; Henzl, M. T.; Rawling, J.; Orme-Johnson, W. H. *Biochim. Biophys. Acta* **1978**, *537*, 185. (b) Huynh, B. H.; Henzl, M. T.; Christner, J. A.; Zimmerman, R.; Rome-Johnson, W. H.; Münck, E. *Biochim. Biophys. Acta* **1980**, *623*, 124.
(5) Münck, E. *Adv. Chem. Ser.* **1981**, 305.
(6) Kanatzidis, M. G.; Baenziger, N. C.; Coucouvanis, D.; Simopoulos, A.; Kostikas, A. *J. Am. Chem. Soc.* **1984**, *106*, 4500.

0002-7863/85/1507-4925$01.50/0

report on I has been published.[7]

Experimental Section

1. Synthesis. The chemicals in this research were used as purchased. Dimethylformamide (DMF) was stored over 4A Linde molecular sieves for 24 h and then distilled under reduced pressure at ~40 °C. Acetonitrile (CH_3CN) was distilled from calcium hydride (CaH_2) before use. Diethyl ether was anhydrous grade and was used without any further purification. The diethyldithiocarbamate trihydrate was purchased from Baker Chemicals. The benzoyl chloride was from Aldrich Chemical Co. Elemental analyses, on samples dried under vacuum for 12 h, were performed by Galbraith Analytical Laboratories, Knoxville, TN.

2. Physical Methods. Visible and ultraviolet spectra were obtained on Cary Model 118 and 219 spectrophotometers. Proton NMR were obtained on JEOL FX90Q and Bruker WM 360 MHz Pulse FT NMR spectrometers with Me_4Si as internal standard. Chemical shifts are reported in parts per million (ppm). The following convention is used whenever isotropically shifted NMR spectra are reported. A negative sign is assigned to a resonance appearing upfield from Me_4Si. A positive sign is given to absorptions occurring downfield from Me_4Si.

Electrochemical measurements were performed with a PAR Model 173 potentiostat/galvanostat and a PAR Model 175 universal programmer. The electrochemical cell used had platinum working and auxiliary electrodes. As reference electrode a saturated calomel electrode was used. All solvents used in the electrochemical measurements were properly dried and distilled, and tetra-*n*-butylammonium perchlorate (Bu_4NClO_4) was used as the supporting electrolyte. Normal concentrations used were ~0.001 M in electroanalyte and 0.1 M in supporting electrolyte. Purified argon was used to purge the solutions prior to the electrochemical measurements. The powder diffraction diagrams were obtained by using a 114-nm diameter Debye–Scherrer-type camera with Ni-filtered Cu Kα radiation (λ = 1.5418 Å).

3. Preparation of Compounds. Bis(tetraphenylphosphonium) Bis(diethyldithiocarbamato)bis(thiophenolato)tetrakis(μ_3-sulfido)tetraferrate(2II,2III) [$[Ph_4P]_2Fe_4S_4(SPh)_2(Et_2Dtc)_2$] (I). Method A. To a solution of 1.10 g (0.83 mmol) of $(Ph_4P)_2Fe_4S_4(SPh)_2Cl_2$[8] in 40 mL of CH_3CN was added 0.40 g (1.78 mmol) of solid $Et_2NCSSNa{\cdot}3H_2O$ while stirring. A color change occurred almost immediately toward brown with an olive green cast to it. After stirring for 20 min, the resulting solution was filtered and 150 mL of anhydrous ethyl ether was added to the filtrate. Upon standing for ca. 3 h, 1.20 g of microcrystalline black material was deposited, isolated, and dried in vacuo, yield, 93%. It can be recrystallized from CH_3CN diethyl ether mixtures yield, 70%.

Anal. Calcd for $Fe_4S_{10}P_2C_{70}N_7H_{70}$ (M_r = 1544); Fe, 14.51; S, 20.73; C, 54.42; N, 1.81; H, 4.53. Found: Fe, 14.68; S, 20.03; C, 55.37; N, 1.88; H, 4.72. Although the analysis of this compound appears satisfactory for the title stoichiometry, Mössbauer NMR and electrochemical results indicate the presence of small but significant amounts of other $[Fe_4S_4(SPh)_n(Et_2Dtc)_{4-n}]^{2-}$ clusters that most likely cocrystallize with the n = 2 compound.

Method B. To a solution of 0.60 g (0.4 mmol) of $(Ph_4P)_2Fe_4S_4(SPh)_4$ in 30 mL of CH_3CN was added a solution of 0.20 g (0.89 mmol) of $Et_2DtcNa{\cdot}3H_2O$ in 20 mL of CH_3cN and the resulting mixture was stirred for 10 min. Following filtration, 130 mL of ethyl ether was added to the solution to induce crystallization. Upon standing for ca. 3 h, 0.50 g of black crystals of $(Ph_4P)_2Fe_4S_4(SPh)_2(Et_2Dtc)_2$ were obtained, yield, 79%. The X-ray powder pattern and all other physical properties of this material were identical with those of the product obtained by method A.

Bis(tetraphenylphosphonium) Dichlorobis(diethyldithiocarbamato)tetrakis(μ_3-sulfido)tetraferrate(2II,2III) [$[Ph_4P]_2Fe_4S_4Cl_2(Et_2Dtc)_2$] (II). Method A. To 30 mL of a CH_3CN solution containing 1.00 g (0.85 mmol) of $(Ph_4P)_2Fe_4S_4Cl_4$ was added 0.42 g (1.87 mmol) of solid $Et_2Dtc{\cdot}Na3H_2O$ while stirring. A color change occurred toward olive green with a brown cast to it. After stirring for ca. 40 min and following filtration to remove NaCl, 150 mL of ethyl ether was added to incipient crystallization. Upon standing for ca. 4 h, 0.95 g of black microcrystalline material was deposited, isolated, and dried in vacuo, yield, 79%. This compound can be recrystallized from CH_3CN, ethyl ether mixtures.

Anal. Calcd for $Fe_4S_8P_2Cl_2C_{58}N_2H_{60}$ (M_r = 1397): Fe, 16.03; S, 18.32; C, 49.82; N, 2.00; H, 4.29. Found: Fe, 16.02; S, 17.74; C, 48.45; N, 1.91; H, 4.33.

Method B. To a 30-mL CH_3CN solution of 0.60 g (0.39 mmol) of $(Ph_4P)_2(Fe_4S_4(SPh)_2(Et_2Dtc)_2)$ was added 0.11 g (0.78 mmol) of PhCOCl dropwise with a syringe. After stirring for ca. 10 min, the resulting solution was filtered and to the filtrate 120 mL of ethyl ether was added. After allowing the solution to stand for ca. 3 h, a black crystalline product formed. It was collected and dried in vacuo: weight, 0.40 g; yield, 74%. The X-ray powder diffraction pattern of this product and its spectroscopic properties were identical with those obtained for the product from method A.

Bis(tetraphenylphosphonium) Trichloro(diethyldithiocarbamato)tetrakis(μ_3-sulfido)tetraferrate(2II,2III) [$[Ph_4P]_2Fe_4S_4Cl_3(Et_2Dtc)$]·DMF (III). To a solution of 1.30 g (1.10 mmol) of $(Ph_4P)_2Fe_4S_4Cl_4$ in 40 mL of CH_3CN was added 20 mL of a solution of 0.25 g (1.11 mmol) of $Et_2DtcNa{\cdot}3H_2O$ and the resulting solution was stirred for 4 min and subsequently filtered. To the olive green filtrate 150 mL of ethyl ether was added to induce crystallization. Upon standing for ca. 4 h, 1.10 g of black crystals were deposited, collected, and dried in vacuo, yield, 86%. They can be recrystallized from DMF ether mixtures.

Anal. Calcd for $Fe_4S_6P_2Cl_3C_{56}N_2OH_{57}$ (MW = 1470): Fe, 16.50; S, 14.14; Cl, 7.84; C, 49.50; N, 2.06; H, 4.20. Found: Fe, 16.26; S, 14.56; Cl, 7.75; C, 48.76; N, 1.37; H, 4.07.

Reaction of $[Ph_4P]_2(Fe_4S_4(Cl)_3(Et_2Dtc))$ with PhCOCl. $[Ph_4P]_2Fe_4S_4(Cl)_3(Et_2Dtc)$, 0.60 g (0.41 mmol), was dissolved in 30 mL of CH_3CN. To this solution 0.06 g (0.40 mmol) of PhCOCl was added via syringe, with stirring. The resulting solution was filtered after ca. 10 min. No apparent color change was observed. To the filtrate 130 mL of diethyl ether was added and the solution was left overnight. Pure black microcrystalline material, 0.43 g, was obtained, yield, 92%. This product was identified by UV/vis spectroscopy and X-ray powder diffraction pattern to be $[Ph_4P]_2Fe_4S_4Cl_4$.[8,9]

Reaction of $[Ph_4P]_2(Fe_4S_4Cl_3(Et_2Dtc))$ with Et_2Dtc^-. $[Ph_4P]_2Fe_4S_4Cl_3(Et_2Dtc)$, 0.85 g (0.63 mmol), was dissolved in ca. 40 mL of CH_3CN. $NaEt_2Ddt{\cdot}3H_2O$, 0.14 g (0.62 mmol), was added to the solution with stirring. After stirring for 15 min, the solution was filtered to remove NaCl and to the olive green filtrate 140 mL of diethyl ether was added. Upon standing overnight, 0.80 g of black microcrystalline product was collected. This product was identical with an "authentic" sample of $[Ph_4P]_2[Fe_4S_4Cl_2(Et_2Dtc)_2]$, yield, 90%.

Reaction of $[Ph_4P]_2Fe_4S_4Cl_2(Et_2Dtc)_2$ with PhCOCl. $[Ph_4P]_2[Fe_4S_4Cl_2(Et_2Dtc)_2]$, 0.85 g (0.63 mmol), was dissolved in ca. 40 mL of CH_3CN. To this olive green solution 0.19 g (1.40 mmol) of PhCOCl was added via syringe and with stirring. After stirring for approximately 20 min, the color of the solution became brown-purplish. Following filtration of the solution, 150 mL of diethyl ether was added and after standing for 2 h 0.68 g of product was obtained. This product was identified by UV/vis spectroscopy to be $[Ph_4P]_2Fe_4S_4Cl_4$, yield, 92%.

4. X-ray Diffraction Measurements. Collection of Data. Single crystals for I–III were obtained by the slow diffusion of diethyl ether into CH_3CN or DMF solutions of the complexes. The crystals used for data collection were sealed in quartz capillaries. Details concerning crystal characteristics are shown in Table I. Intensity data for the $[Ph_4P]^+$ salts of $[Fe_4S_4(SPh)_2(Et_2Dtc)_2]^{2-}$, $[Fe_4S_4Cl_2(Et_2Dtc)_2]^{2-}$, and $[Fe_4S_4Cl_3(Et_2Dtc)]^{2-}$ were obtained on a Nicolet P3/F four-circle diffractometer. A detailed description of the instrument and the data acquisition procedures have been described earlier.[10] The cell dimensions for I–III were refined using 20–25 machine-centered reflections with 2θ values between 25° and 40° (Mo Kα_1, λ = 0.709 26 Å).

Reduction of Data. The raw data were reduced to net intensities, estimated standard deviations were calculated on the basis of counting statistics, Lorentz–polarization corrections were applied, and equivalent reflections were averaged. The estimated standard deviation of the structure factor was taken as the larger of that derived from counting statistics and that derived from the scatter of multiple measurements.

The least-squares program used minimizes $\sum w(\Delta|F|)^2$. The weighting function used throughout the refinement of the structure gives zero weight to those reflections with $F^2 \leq 3\sigma(F^2)$ and $w = 1/\sigma^2(F)$ to all others $[\sigma^2(F^2) = (0.06F^2)^2 + \sigma^2(F^2)$ (from counting statistics)].[11]

The scattering factors of the neutral non-hydrogen atoms were taken from the tables of Doyle and Turner,[12] and real and imaginary dispersion corrections[13] were applied to all of them. The spherical hydrogen scattering factor tables of Stewart, Davidson, and Simpson[14] were used. In view of the small values of μ (Table I) no absorption correction was applied to any of the three data sets.

Determination of Structures. $[Ph_4P]_2[Fe_4S_4(SPh)_2(Et_2Dtc)_2]$ (I). The structure of I was initially determined by using data collected with $2\theta_{max}$

(7) Kanatzidis, M. G.; Ryan, M.; Coucouvanis, D.; Simopoulos, A.; Kostikas, A. *Inorg. Chem.* **1983**, *22*, 179.

(8) Coucouvanis, D.; Kanatzidis, M.; Simhon, E.; Baenziger, N. C. *J. Am. Chem. Soc.* **1982**, *104*, 1874.

(9) Bobrik, M. A.; Hodgson, K. O.; Holm, R. H. *Inorg. Chem.* **19778** *16*, 1851.

(10) Kanatzidis, M. G.; Coucouvanis, D. *Inorg. Chem.* **1984**, *23*, 403.

(11) Grant, D. F.; Killean, R. C. G.; Lawrence, J. L. *Acta Crystallogr., Sect. B* **1969**, *B25*, 374.

(12) Doyle, P. A.; Turner, P. S. *Acta Crystallogr., Sect. A* **1968**, *A24*, 390.

(13) Cromer, D. T.; Liberman, D. *J. Chem. Phys.* **1970**, *53*, 1891.

(14) Stewart, R. F.; Davidson, E. R.; Simpson, W. T. *J. Chem. Phys.* **1965**, *42*, 3175.

Table I. Summary of Crystal Data, Intensity Collection, Solution, and Refinement

	$(Ph_4P)_2Fe_4S_4(SPh)_2(Et_2Dtc)_2$	$(Ph_4P)_2Fe_4S_4(Cl)_2(Et_2Dtc)_2$	$(Ph_4P)_2Fe_4S_4Cl_3(Et_2Dtc)\cdot DMF$
formula	$Fe_4S_{10}P_2C_{70}N_2H_{70}$	$Fe_4S_8P_2Cl_2C_{58}N_2H_{60}$	$Fe_4S_6P_2Cl_3C_{56}N_2OH_{57}$
M_r	1544	1397	1357.5
a, Å	17.486 (3)	20.409 (6)	15.836 (2)
b, Å	18.240 (3)	13.873 (3)	17.803 (2)
c, Å	24.198 (3)	25.739 (9)	22.496 (3)
α, deg	90.00	90.00	90.00
β, deg	109.73 (1)	118.94 (2)	101.44 (1)
γ, deg	90.00	90.00	90.00
Z, V, Å^3	4, 7163.2	4, 6378	4, 6216
d_{calcd}, g/cm^3	1.41	1.45	1.45
d_{obsd}, g/cm^3 [a]	1.40	1.43	1.45
space group	$C2/c$	$C2/c$	$P2_1/c$
cryst dimens, mm	1.16 × 0.22 × 0.22	0.52 × 0.30 × 0.12	0.48 × 0.22 × 0.07
radiatn	Mo ($\lambda_{K\alpha}$) 0.71069 Å	Mo ($\lambda_{K\alpha}$) 0.71069 Å	Mo ($\lambda_{K\alpha}$) 0.71069 Å
abs coeff μ, cm^{-1}	11.6	13.14	13.5
data collected	2θ = 50°, $h,k,\pm l$	2θ = 40°, $h,k,\pm l$	2θ = 45°, $h,k,\pm l$
unique data	5941	3058	8392
data used in refinement $F_o^2 3(F_o^2)$	3226	1919	5038
no. of atoms in asym unit	79	68	131
no. ov variables	661	343	402
scan speed min, max	6.00, 29.3	4.59, 29.30	4.35, 29.30
phasing technique	direct methods	direct methods	direct methods
R, %	7.94	5.63	5.11
R_w, %	10.70	6.15	6.90

[a] Determined by flotation in a CCl_4/pentane mixture.

= 40°. The $[Fe_4S_4(SPh)_2(Et_2Dtc)_2]^{2-}$ anion is required by symmetry to reside on a crystallographic 2-fold axis. Two iron and two sulfur atoms belonging to the Fe_4S_4 core were located initially by using the direct methods program MULTAN.[15]

The remaining non-hydrogen atoms were located by subsequent Fourier syntheses following least-squares refinement of the input atomic coordinates. The refinement of all atoms in the asymmetric unit using isotropic temperature factors and the limited data set gave an R value of 0.16. Further refinement using additional data ($40 < 2\theta < 50$) and anisotropic temperature factors on all the atoms converged to an R value of 0.084. At this stage, the hydrogen atom positions were calculated (C–H, 0.95 Å) and included in the structure factor calculation but were not refined. The final R value was 0.079 and the weighted R_w was 0.107. During the last cycle of refinement, all parameter shifts were less than 10% of their esd's.

$[Ph_4P]_2[Fe_4S_4Cl_2(Et_2Dtc)_2]$ (II). The structure of II was solved by the direct methods routine SOLV of the SHELXTL[16] crystallographic package. Here too the anion $(Fe_4S_4Cl_2(Et_2Dtc)_2)^{2-}$ is required by symmetry to reside on a crystallographic 2-fold axis. After the heavy atom fragment of the structure was located, the rest of the non-hydrogen atoms were found from subsequent Fourier electron density difference maps. Refinement of all atoms after several cycles converged to an R value of 0.096. At this point all the atoms were assigned anisotropic temperature factors and further refinement resulted to R = 0.065. At this point the hydrogen atom coordinates were calculated and the hydrogen atoms were input in the structure factor calculations but were not refined. In the final cycle of refinement, using anisotropic temperature factors for all non-hydrogen atoms, the final R value was 0.056. The weighted R was 0.061 and all parameter shifts were less than 10% of their esd.

$[Ph_4P]_2[Fe_4S_4Cl_3(Et_2Dtc)]\cdot DMF$ (III). The structure of III was solved by the direct methods procedure using the program MULTAN.[15] The anion is sitting on a general position. The Fe_4S_4 fragment was located and its position was verified by a three-dimensional Patterson synthesis map. The eight "heavy" atoms phased the subsequent electron density map sufficiently well to allow the location of virtually all the atoms in the structure. Isotropic refinement of all the non-hydrogen atoms converged to an R value of 0.11. At this stage, the position of the DMF molecule of solvation was revealed. Further refinement was not attempted due to poor quality of a certain class of reflections ($5,k,l$ to $10,k,l$) probably because of gross crystal misallignment. A second data set was collected ($2\theta_{max}$ = 45°) and used for further refinement. The new data gave R = 0.077. When the refinement was continued with anisotropic temperature factors assigned only to the anion non-hydrogen atoms and the phosphorus atoms of the cation, the structure converged after four cycles to R = 0.056. At this stage the hydrogen atoms were included in the structure factor calculation at their calculated positions but were not refined (C–H, 0.95 Å). A final cycle of least-squares refinement resulted in values of R_w = 0.069 and R = 0.051.

Table II. Positional Parameters and Standard Deviations for the Non-Hydrogen Atoms $[Fe_4S_4(SPh)_2(Et_2Dtc)_2]^{2-}$

atom	X	Y	Z
Fe(1)	0.07096 (9)	0.02163 (8)	0.72669 (8)
Fe(2)	−0.05351 (8)	−0.08134 (9)	0.69378 (7)
S(1)	−0.0701 (2)	0.0384 (2)	0.6789 (2)
S(2)	−0.1276 (2)	−0.8991 (1)	0.7218 (1)
S(t)	−0.1276 (2)	−0.1411 (3)	0.6100 (2)
S(1DT)	−0.2192 (2)	0.0615 (2)	0.7445 (2)
S(2DT)	−0.0952 (2)	0.860 (2)	0.8541 (2)
N	−0.2492 (7)	0.1092 (7)	0.8380 (6)
C(1DT)	−0.1935 (7)	0.0851 (7)	0.8166 (6)
C(ST1)	0.409 (1)	0.275 (1)	0.6038 (9)
C(ST2)	0.365 (1)	0.238 (1)	0.547 (1)
C(ST3)	0.386 (3)	0.179 (2)	0.544 (2)
C(ST4)	0.448 (2)	0.137 (1)	0.571 (1)
C(ST5)	0.498 (2)	0.174 (1)	0.627 (1)
C(ST6)	0.481 (2)	0.239 (1)	0.644 (1)
C(2DT)	−0.227 (1)	0.125 (1)	0.903 (1)
C(3DT)	−0.343 (1)	0.114 (1)	0.801 (1)
C(4DT)	−0.351 (2)	0.185 (2)	0.772 (1)
C(5DT)	−0.232 (1)	0.061 (1)	0.939 (1)

Table III. Positional Parameters and Standard Deviations for the Non-Hydrogen Atoms $[Fe_4S_4Cl_2(Et_2Dtc)_2]^{2-}$

atom	X	Y	Z
Fe(1)	0.58382 (9)	0.2716 (1)	0.27227 (7)
Fe(2)	0.5100 (1)	0.4104 (1)	0.30717 (7)
S(1)	0.6001 (2)	0.4356 (2)	0.2792 (1)
S(2)	0.4886 (2)	0.2506 (2)	0.1774 (1)
C(1)	0.5299 (2)	0.4999 (3)	0.3864 (2)
S(1DT)	0.6680 (2)	0.1547 (3)	0.3429 (2)
S(2DT)	0.6912 (2)	0.2338 (3)	0.2500 (2)
N	0.7839 (6)	0.1045 (8)	0.3281 (5)
C(1DT)	0.7212 (7)	0.161 (1)	0.3097 (5)
C(2DT)	0.8275 (9)	0.101 (1)	0.2964 (7)
C(3DT)	0.884 (1)	0.177 (1)	0.3152 (9)
C(4DT)	0.810 (1)	0.045 (1)	0.3804 (8)
C(5DT)	0.853 (1)	0.092 (2)	0.4343 (9)

Crystallographic Results. The final atomic positional and thermal parameters of the non-hydrogen atoms in $(Ph_4P)_2[Fe_4S_4(SPh)_2(Et_2Dtc)_2]$, $(Ph_4P)_2[Fe_4S_4(Et_2Dtc)_2Cl_2]$, and $(Ph_4P)_2[Fe_4S_4(Et_2Dtc)Cl_3]\cdot DMF$ with standard deviations derived from the inverse matrices of the least-squares refinements are compiled in Tables II, III and IV,

(15) Main, P.; Wollfson, M. M.; Germain, G. "MULTAN: A Computer Program for the Automatic Solution of Crystal Structures"; University of York: York, England, 1971.

(16) SHELXTL package of Crystallographic Programs, Nicolet XRD Corporation, Fremont, CA.

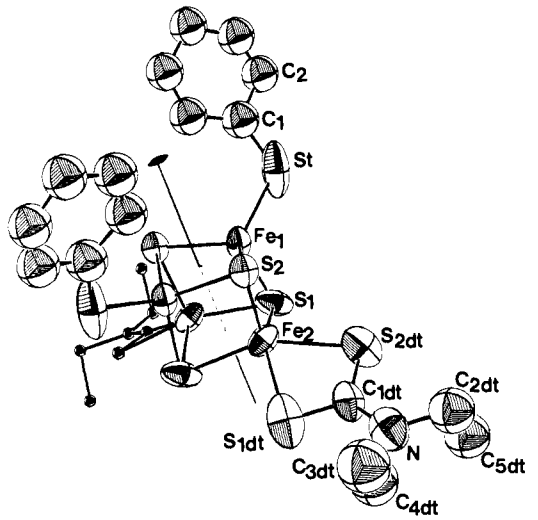

Figure 1. Crystal structure of the $[Fe_4S_4(SPh)_2(Et_2Dtc)_2]^{2-}$ anion showing the atom labeling scheme. Thermal ellipsoids are drawn by ORTEP (Johnson, C. K. Report ORNL-3794, Oak Ridge National Laboratory, Oak Ridge, TN, 1965) and represent 50% probability surfaces. The ellipsoids for one of the Et_2Dtc ligands have been drawn artificially small for clarity.

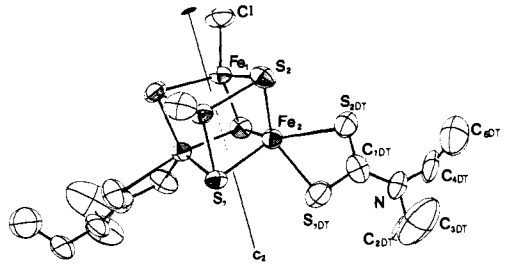

Figure 2. Structure of the $[Fe_4S_4Cl_2(Et_2Dtc)_2]^{2-}$ anion showing the atom labeling scheme. Drawn by ORTEP.

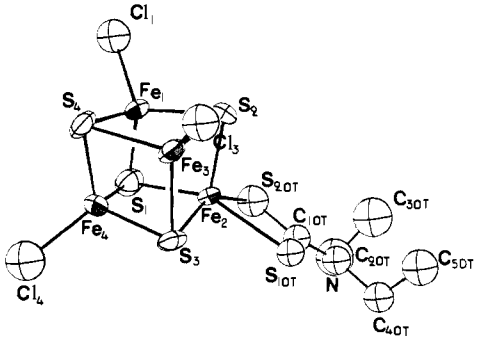

Figure 3. Structure of the $[Fe_4S_4Cl_3(Et_2Dtc)]^{2-}$ anion showing the atom labeling scheme. Drawn by ORTEP.

respectively. Intramolecular distances and angles for the anions in I and II are given in Table V and for the anion in III in Table VI. The structures and atom labeling schemes are shown in Figures 1–3.

Results and Discussion

1. Synthesis of Clusters. The previously reported $[Fe_4S_4(SPh)_2Cl_2]^{2-}$[6,8] and the known $(Fe_4S_4Cl_4)^{2-}$[8,9] clusters were used as starting materials in the synthesis of the $[Fe_4S_4(X)_n(Et_2Dtc)_{4-n}]^{2-}$ clusters,[17] using simple metathetical reactions of the type

$$[Fe_4S_4(X)_nCl_{4-n}]^{2-} + n\,NaEt_2Dtc \rightarrow [Fe_4S_4(X)_{4-n}(Et_2Dtc)_n]^{2-} + n\,NaCl\downarrow \quad (1)$$

$$X = SPh, Cl;\ n = 1, 2$$

(17) Et_2Dtc : diethyldithiocarbamate: $(C_2H_5)_2NCS_2^-$.

Table IV. Positional Parameters and Standard Deviations for the Non-Hydrogen Atoms in $[Fe_4S_4Cl_3(Et_2Dtc)]^{2-}$

atom	X	Y	Z
Fe(1)	0.19145 (7)	0.24028 (6)	0.30526 (5)
Fe(2)	0.32860 (7)	0.24473 (6)	0.24035 (5)
Fe(3)	0.34079 (7)	0.32936 (7)	0.34947 (5)
Fe(4)	0.22782 (8)	0.38137 (6)	0.24883 (5)
S(1)	0.1783 (1)	0.2696 (1)	0.20508 (8)
S(2)	0.3272 (1)	0.2012 (1)	0.33558 (9)
S(3)	0.3746 (1)	0.3703 (1)	0.2621 (1)
S(4)	0.2013 (1)	0.3703 (1)	0.34376 (9)
P(1)	−0.1085 (1)	0.3819 (1)	0.41894 (9)
P(2)	0.3032 (1)	−0.0373 (1)	0.4724 (1)
C(11)	0.0927 (2)	0.1794 (1)	0.3383 (1)
C(13)	0.4242 (2)	0.3666 (1)	0.4363 (1)
C(14)	0.1764 (2)	0.4816 (1)	0.1956 (1)
S(1DT)	0.4722 (1)	0.2178 (2)	0.2183 (1)
S(2DT)	0.3151 (1)	0.1397 (1)	0.1668 (1)
N	0.4664 (4)	0.1061 (4)	0.1377 (3)
C(1DT)	0.4241 (5)	0.1474 (5)	0.1707 (3)
C(2DT)	0.5602 (7)	0.1220 (7)	0.1357 (6)
C(3DT)	0.615 (1)	0.0740 (9)	0.1770 (7)
C(4DT)	0.4243 (6)	0.0472 (6)	0.0964 (4)
C(5DT)	0.4114 (7)	−0.0259 (7)	0.1273 (5)

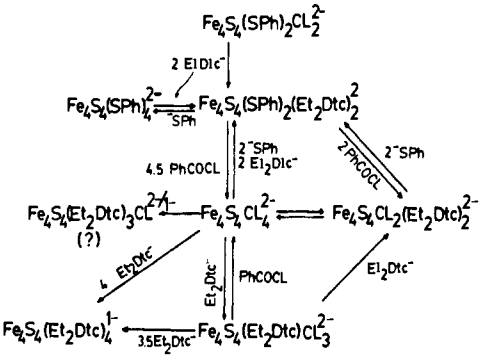

Figure 4. Synthesis and interconversions of $[Fe_4S_4(X)_n(Et_2Dtc)_{4-n}]^{2-}$ clusters.

The Ph_4P^+ salts of these air-sensitive anions were obtained pure in crystalline form in yields >79%. The $[Fe_4S_4(SPh)_4(Et_2Dtc)_2]^{2-}$ complex I also can be obtained by the reaction of $(Ph_4P)_2Fe_4S_4(SPh)_4$ with $NaEt_2Dtc$ in CH_3CN under similar reaction conditions. The conversion of I to $[Fe_4S_4(Cl)_2(Et_2Dtc)_2]^{2-}$ II by the reaction of the former with 2 equiv of PhCOCl is accomplished readily. Similar interconversions between I, II, and III can be accomplished with appropriate reactants. These reactions (Figure 4) can be monitored spectrophotometrically and proceed to yields >90%.

The $[Fe_4S_4Cl(Et_2Dtc)_3]^{2-}$ complex is the only member of the series (eq 1, $n = 3$) that could not be obtained in pure crystalline form. It was found to be contaminated with $[Fe_4S_4(Et_2Dtc)_4]^{1-}$[18] and possibly $[Fe_4S_4Cl(Et_2Dtc)_3]^{1-}$. The difficulty in obtaining this member of the series could be explained in terms of the electrochemical behavior of the species (vide infra).

The electronic spectra of the mixed ligand clusters (in CH_3CN) are as follows: I, 420 nm (ϵ 12 500); II, 680 nm (ϵ 1042); III, 680 nm (ϵ 1342), 500 (sh). The spectra resemble those of the corresponding $[Fe_4S_4(L)_4]^{2-}$ (L = SPh, Cl) cubanes,[19,9] only with smaller molar absorptivities. No absorption could be detected that could directly be attributed to Et_2Dtc^- coordination (Figure 5).

2. Crystallographic Studies. Description of the Structures of the $(Ph_4P)_2[FeS_4(X)_2(Et_2Dtc)_2]$ [X = SPh (I); X = Cl (II)] Complexes. The crystal structures of I and II consist of discrete cations and anions. The cations have their expected unexceptional

(18) $[Ph_4P]Fe_4S_4(Et_2Dtc)_4$: Coucouvanis, D.; Kanatzidis, M. G.; Wickman, H. H.; Simopoulos, A.; Kostikas, A., unpublished results.

(19) Que, L.; Bobrik, M. A.; Ibers, J. A.; Holm, R. H. *J. Am. Chem. Soc.* **1974**, *96*, 4168.

Table V. Selected Distances (Å) and Angles in the Anions[a] of the Ph_4P^+ Salts of $[Fe_4S_4(SPh)_2(Et_2Dtc)_2]^{2-}$ (I) and $[Fe_4S_4Cl_2(Et_2Dtc)_2]^{2-}$ (II) Other Than Those Listed in Table VII

	I	II
S(1)–S(1)′	3.485 (8)	3.533 (7)
S(2)–S(2)′	3.635 (6)	3.616 (6)
S(1)–S(2)	3.562 (4)	3.585 (4)
S(1)–S(2)′	3.594 (4)	3.615 (4)
mean[b]	3.569 (30)	3.587 (20)
S(1DT)–S(1)′	3.305 (5)	3.268 (5)
S(2DT)–S(1)	3.362 (5)	3.637 (5)
S(1DT)–S(2)	3.705 (5)	3.635 (5)
S(2DT)–S(2)	3.908 (5)	4.191 (5)
S(1DT)–S(2DT)	2.837 (6)	2.871 (5)
S(T)–C(1)	1.690 (28)	
S(1DT)–C(1DT)	1.703 (13)	1.682 (14)
S(2DT)–C(1DT)	1.651 (12)	1.681 (13)
C(1DT)–N	1.325 (14)	1.379 (15)
N–C(2DT)	1.524 (22)	1.446 (18)
N–C(3DT)	1.575 (21)	1.472 (17)
S(T)–Fe(1)–S(2)	118.75 (16)	117.03 (18)
S(T)–Fe(1)–S(2)′	114.33 (16)	112.19 (17)
S(T)–Fe(1)–S(1)	108.86 (21)	113.74 (17)
S(1)–Fe(1)–S(2)	105.54 (17)	105.13 (16)
S(1)–Fe(1)–S(2)′	103.85 (17)	104.07 (15)
mean[b]	110 (3)	110 (3)
S(2DT)–Fe(2)–S(1)	88.90 (15)	85.13 (14)
S(2DT)–Fe(2)–S(1DT)	69.27 (17)	70.02 (14)
S(1DT)–Fe(2)–S(1)′	92.13 (17)	96.56 (14)
S(2DT)–Fe(2)–S(1)′	142.21 (22)	130.16 (16)
S(1DT)–Fe(2)–S(1)	153.18 (18)	154.99 (17)
S(2DT)–Fe(2)–S(2)	112.80 (16)	125.54 (17)
S(1DT)–Fe(2)–S(2)	100.67 (15)	96.56 (15)
S(2DT)–Fe(2)–S(1)	102.17 (18)	103.04 (15)
Fe(1)–S(2)–Fe(1)′	72.83 (10)	73.82 (12)
Fe(1)–S(2)–Fe(2)	75.30 (09)	76.46 (11)
Fe(1)′–S(2)–Fe(2)	75.05 (10)	74.72 (11)
Fe(2)′–S(1)–Fe(2)	81.57 (12)	80.74 (12)
Fe(1)–S(1)–Fe(2)	75.71 (11)	75.83 (10)
Fe(1)–S(1)–Fe(2)′	74.65 (11)	75.22 (10)
mean	75 (1)	76 (1)
S(1DT)–C(1DT)–S(2DT)	115.33 (44)	117.21 (54)
Fe(2)–S(1DT)–C(1DT)	84.26 (37)	83.78 (48)
Fe(2)–S(2DT)–C(1DT)	89.15 (45)	88.95 (51)
S(1DT)–C(1DT)–N	120.72 (79)	121.54 (73)
S(2DT)–C(1DT)–N	123.27 (75)	121.08 (75)

[a] For the cation in I, $[(C_6H_5)_4P]_2[Fe_4S_4(SPh)_2(Et_2Dtc)_2]$, the four P–C bonds are within the range 1.780 (11)–1.804 (10) Å with a mean value of 1.789 (10) Å. The C–C bonds are within the range 1.297 (22)–1.488 (23) Å with a mean value of 1.376 (45) Å. The six C(*i*)–P–C(*j*) angles are found between 106.6 (6)° and 112.0 (6)° with a mean value of 109 (2)°. The C–C–C angles are in the range 118.04 (4)–122.9 (7)° with a mean value of 120 (2)°. For the cations scatter estimate has been obtained as follows: $s = [\sum_{i=1}^{N}(X_i - \bar{X})^2/(N-1)]^{1/2}$ where X_i is the value of an individual bond or angle and $\bar{X}$ is the mean value for the N equivalent bond lengths or angles. Intermolecular H contacts shorter than 2.82 Å were not found. For the cation in II, $[(C_6H_5)_4P]_2[Fe_4S_4(Et_2Dtc)_2Cl_2]$, the four P–C bonds are within the range 1.790 (12–1.808 (12) Å with a mean value of 1.797 (10) Å. The C–C bonds are in the range 1.32 (2)–1.40 (2) Å with a mean value of 1.38 (3) Å. The six C(*i*)–P–C(*j*) angles are found between 108.4 (1)° and 111.7 (1)° with a mean value of 109 (2)°. The C–C–C angles range from 122.7 (0.7)° to 117.4 (0.7)° with a mean value of 120 (1.4)°. [b] The standard deviation from the mean, σ, is reported. $\sigma = [\sum_{i=1}^{N}(X_i - \bar{x})^2/N(N-1)]^{1/2}$.

geometry and will not be considered further. Selected atomic distances and angles are compiled in Table V. A comparison of the structural parameters in I and II to those in III, $[Fe_4S_4(SPh)_2Cl_2]^{2-}$, and $[Fe_4S_4(S_2C_2(CF_3)_2)_4]^{2-}$ is shown in Table VII.

In the crystal structures of I and II, the $[Fe_4S_4(X)_2(Et_2Dtc)_2]^{2-}$ anions (X = PhS^-, Cl^-) are located on crystallographic 2-fold axes which pass through the midpoints of the opposite faces (Fe(1)-Fe(1)′S(2)S(2)′ and Fe(2)Fe(2)′S(1)S(1)′) of the distorted Fe_4S_4 cubes. Unlike the Fe_4S_4 cores in the $[Fe_4S_4(L)_4]^{2-}$ clusters (L = SPh,[19] SCH_2Ph,[20] Cl^-[9]) which show approximate D_{2d} symmetry, the Fe_4S_4 cores in I and II do not show any approximate symmetry higher than the crystallographically imposed C_2 symmetry (Table VII).

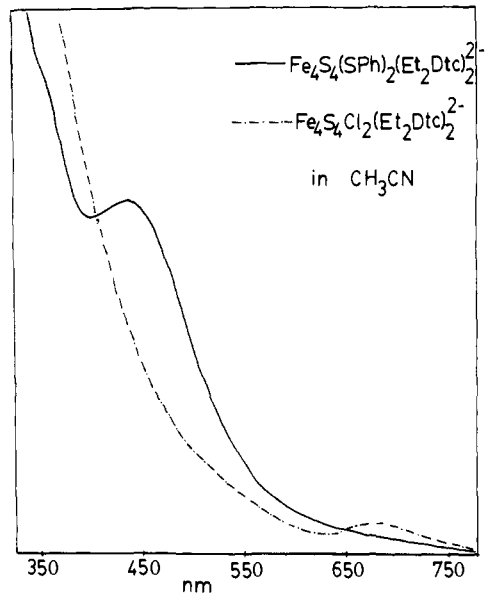

Figure 5. Electronic spectra of $[Fe_4S_4(SPh)_2(Et_2Dtc)_2]^{2-}$ and $[Fe_4S_4Cl_2(Et_2Dtc)_2]^{2-}$ clusters in CH_3CN.

The Fe_4S_4 units in I and II contain two structurally distinct iron sites. One of the sites has tetrahedrally coordinated iron atoms with PhS^- and Cl^- terminal ligands for I and II, respectively. The $S_3Fe(SPh)$ and S_3FeCl coordination units and the terminal Fe–S and Fe–Cl distances in I and II are very similar to the ones found in the symmetrically coordinated $[Fe_4S_4(L)_4]^{2-}$ clusters (L = SPh,[19] Cl^-[9]). The second site is rather uncommon and shows the iron atoms coordinated by the Et_2Dtc[17] chelating ligands. As a consequence the Fe atoms in these sites show a distorted square-pyramidal FeS_5 coordination. The clusters I and II represent the first examples of $[Fe_4S_4]^{2+}$ cores that contain square-pyramidal five-coordinate (FeS_5) iron sites. The S(1dt), S(2dt), S(1), and S(1)′ atoms in I (Figure 1) are coplanar. The four S(2)–Fe(2)–S_{eq} angles in I range from 96.44° to 112.80° with a mean value of 103.2 (3.5)° and the iron is out of the equatorial S(1dt)–S(2dt)–S(1)–S(1)′ plane by 0.59 Å. By contrast, the corresponding S(1dt), S(2dt), S(1), and S(1)′ basal atoms in II deviate from planarity. The four S atoms depart from the best least-squares plane by −0.41, +0.36, −0.27, and +0.33 Å, respectively. The Fe(2) atom is elevated from that plane by 0.62 Å. The S(1)–Fe(2)–S_{eq} angles in II vary from 96.56° to 125.54° with a mean value of 105.6 (3.5)°. By comparison with I and II the $\overline{Cl\text{–}Fe\text{–}S}$ angle in the square-pyramidal $Cl\text{–}Fe(Et_2Dtc)_2$ complex[21] is 105.4 (3.0)° and the iron is above the basal plane by 0.62 Å. The Fe(2)–S(2) vectors in I and II deviate from the normal to the equatorial planes by 5° and 6°, respectively. The disposition of the Et_2Dtc ligand in II results in a FeS_5 polyhedron that could also be regarded as an intermediate between a square pyramid and a trigonal bipyramid.

The Et_2Dtc ligands in the two anions can assume different orientations. It is evident that the S(1dt)–C(1dt)–S(2dt) ligand plane in II (Figure 2) is tilted by 15.5° relative to the theoretical least-squares equatorial plane. In I this tilt is ~1°. This difference in ligand orientation in the two anions can be viewed as a partial rotation of the Et_2Dtc ligands around the Fe(2)–C(1dt) vectors (Figures 1 and 2). In view of the similar electronic structures of I and II, it is reasonable to assume that electronic structure requirements do not dictate any preferred ligand orientation

(20) Averill, B. A.; Herskovitz, T.; Holm, R. H.; Ibers, J. A. *J. Am. Chem. Soc.* **1973**, *95*, 3523.
(21) Hoskins, B. F.; White, A. H. *J. Chem. Soc. A* **1970**, 1668.

Table VI. Selected Distances (Å) and Angles in the Anion[a] of the Ph_4P^+ Salt of $[Fe_4S_4Cl_3(Et_2Dtc)]^{2-}$ (III)

Fe(1)–Fe(3)	2.762 (2)	S(1DT)–S(2)	3.838 (4)	Fe(1)–S(2)	2.296 (2)
Fe(1)–Fe(4)	2.771 (2)	S(2DT)–S(2)	3.920 (4)	Fe(1)–S(4)	2.300 (2)
Fe(3)–Fe(4)	2.752 (2)	S(1DT)–S(3)	3.366 (3)	Fe(2)–S(1)	2.395 (2)
mean[b]	2.762 (6)	S(2DT)–S(1)	3.394 (3)	Fe(2)–S(3)	2.372 (2)
		S(1DT)–S(2DT)	2.884 (3)	Fe(3)–S(2)	2.307 (2)
Fe(2)–Fe(1)	2.849 (2)			Fe(3)–S(4)	2.305 (2)
Fe(2)–Fe(3)	2.854 (2)	Fe(2)–S(1DT)	2.469 (3)	Fe(4)–S(1)	2.288 (2)
Fe(2)–Fe(4)	2.936 (2)	Fe(2)–S(2DT)	2.478 (2)	Fe(4)–S(3)	2.293 (2)
mean	2.88 (3)			mean	2.319 (14)
		Fe(1)–S(1)	2.248 (2)	mean of 12	2.301 (12)
S(1)–S(2)	3.593 (3)	Fe(2)–S(2)	2.282 (2)		
S(1)–S(3)	3.597 (3)	Fe(3)–S(3)	2.259 (2)	S(1DT)–C(1DT)	1.725 (8)
S(1)–S(4)	3.554 (3)	Fe(4)–S(4)	2.265 (2)	S(2DT)–C(1DT)	1.717 (8)
S(2)–S(4)	3.636 (3)	mean (4)	2.263 (7)	C(1DT)–N	1.317 (10)
S(2)–S(3)	3.585 (3)				
S(3)–S(4)	3.594 (3)			Fe(1)–Cl(1)	2.249 (2)
mean	3.593 (11)			Fe(3)–Cl(3)	2.231 (2)
				Fe(4)–Cl(4)	2.213 (2)
				mean	2.231 (10)
Fe(1)–S(1)–Fe(4)	75.30 (7)	Fe(2)–Fe(1)–Fe(3)	61.12 (4)	Cl(1)–Fe(1)–S(1)	119.05 (11)
Fe(2)–S(1)–Fe(4)	77.61 (7)	Fe(2)–Fe(1)–Fe(4)	62.98 (4)	Cl(1)–Fe(1)–S(2)	111.10 (11)
Fe(1)–S(1)–Fe(2)	75.64 (7)	Fe(3)–Fe(1)–Fe(4)	59.66 (4)	Cl(1)–Fe(1)–S(4)	113.38 (10)
Fe(1)–S(2)–Fe(3)	73.76 (7)	Fe(1)–Fe(2)–Fe(3)	57.94 (4)	Cl(3)–Fe(3)–S(2)	115.79 (11)
Fe(1)–S(2)–Fe(2)	76.97 (7)	Fe(1)–Fe(2)–Fe(4)	57.21 (4)	Cl(3)–Fe(3)–S(3)	117.74 (12)
Fe(2)–S(2)–Fe(3)	76.90 (7)	Fe(3)–Fe(2)–Fe(4)	56.74 (4)	Cl(3)–Fe(3)–S(4)	110.41 (11)
Fe(2)–S(3)–Fe(3)	76.05 (7)	Fe(1)–Fe(3)–Fe(2)	60.94 (4)	Cl(4)–Fe(4)–S(1)	114.25 (12)
Fe(3)–S(3)–Fe(4)	74.71 (7)	Fe(1)–Fe(3)–Fe(4)	60.32 (4)	Cl(4)–Fe(4)–S(3)	113.23 (12)
Fe(2)–S(3)–Fe(4)	77.99 (7)	Fe(2)–Fe(3)–Fe(4)	63.13 (4)	Cl(4)–Fe(4)–S(4)	117.59 (12)
Fe(1)–S(4)–Fe(3)	73.72 (7)	Fe(1)–Fe(4)–Fe(2)	59.82 (4)	mean	115 (1)
Fe(1)–S(4)–Fe(4)	74.73 (7)	Fe(1)–Fe(4)–Fe(3)	60.02 (4)		
Fe(3)–S(4)–Fe(4)	74.07 (7)	Fe(2)–Fe(4)–Fe(3)	60.12 (4)	S(1DT)–Fe(2)–S(3)	88.09 (9)
mean	76.5 (4)	mean	60.0 (6)	S(1DT)–Fe(2)–S(2)	107.68 (11)
				S(2DT)–Fe(2)–S(1)	88.29 (8)
		S(1)–Fe(1)–S(2)	104.53 (10)	S(2DT)–Fe(2)–S(2)	110.79 (10)
		S(1)–Fe(1)–S(4)	102.80 (10)	S(2DT)–Fe(2)–S(3)	146.21 (11)
		S(2)–Fe(1)–S(4)	104.60 (10)	S(1DT)–Fe(2)–S(1)	149.69 (11)
		S(1)–Fe(2)–S(2)	100.35 (10)	S(1DT)–Fe(2)–S(2DT)	71.33 (8)
		S(1)–Fe(2)–S(3)	97.96 (10)		
		S(2)–Fe(2)–S(3)	100.74 (10)		
		S(2)–Fe(3)–S(3)	103.48 (10)		
		S(3)–Fe(3)–S(4)	103.87 (10)		
		S(2)–Fe(3)–S(4)	104.06 (10)		
		S(1)–Fe(4)–S(3)	103.47 (10)		
		S(1)–Fe(4)–S(4)	102.61 (10)		
		S(3)–Fe(4)–S(4)	104.06 (10)		
		mean	103.0 (6)		

[a] For the cation in I, $[(C_6H_5)_4P]_2[Fe_4S_4(Et_2Dtc)Cl_3]$, the four P–C bonds are within the range 1.780 (7)–1.809 (8) Å with a mean value of 1.791 (10) Å. The C–C bonds are within the range 1.314 (11)–1.413 (16) Å with a mean value of 1.363 (20) Å. The six C(i)–P–C(j) angles are found between 107.4 (4)° and 111.7 (4)° with a mean value of 109 (2)°. The C–C–C angles are in the range 119.0 (1)–121.2 (1)° with a mean value of 120 (2)°. For the cations scatter estimate has been obtained as follows: $S = [\sum_{i=1}^{N}(X_i - \bar{X})^2/(N-1)]^{1/2}$ where X_i is the value of an individual bond or angle and $\bar{X}$ is the mean value for the N equivalent bond lengths or angles. Intermolecular H contacts shorter than 2 Å were not found. [b] The standard deviation from the mean, σ, is reported. $\sigma = [\sum_{i=1}^{N}(X_i - \bar{x})^2/N(N-1)]^{1/2}$.

relative to the equatorial S(1dt)–S(2dt)–S(1)–S(1)′ plane but rather allow a certain degree of orientation flexibility for the Et_2Dtc^- ligands within the $[Fe_4S_4(X)_2(Et_2Dtc)_2]^{2-}$ anions.

Apart from this difference of the Et_2Dtc orientation, the structural similarities between I and II are apparent. The equatorial Fe(2)–S bonds show unequal lengths in the range 2.309 (4)–2.552 (4) Å in I and 2.288 (4)–2.578 (4) Å in II. A comparison of corresponding distances in I and II are shown in Tables V and VII. The Fe(2)–S(Et_2Dtc) bonds in both anions are significantly longer than the Fe(III)–S bonds in $ClFe(Et_2Dtc)_2$[21] [2.300 (10) Å] but only slightly longer than the Fe(II)–S bonds in the $[Fe_2(Et_2Dtc)_4]$ dimer[22] [2.404 (2) and 2.453 (2) Å]. The Fe(2)–S(Et_2Dtc) bonds in I and II are quite similar to the Fe(III)–S bonds in [Fe(Salen)(PyrrolDtc)][23] [2.452 (2) and 2.566 (2) Å]. It has been suggested[23] that in the latter both sulfur atoms of the $PyrrolDtc^-$ ligand may occupy one coordination site. A similar suggestion could be advanced for the Et_2Dtc^- ligands in I and II.[24]

A closer look at the $[Fe_4S_4]^{2+}$ cores in I and II reveals that they both are highly distorted by comparison to conventional Fe_4S_4 cores.[25] The major feature of the distortion, immediately apparent, is the long Fe–Fe distances [3.053 (3) Å in I and 3.045 (3) Å in II] between the iron atoms [Fe(2)] that are coordinated by the Et_2Dtc ligands. The Fe–Fe distances in both I and II divide into three sets (1 + 1 + 4). The two edges of the Fe_4 tetrahedron that are perpendicular to the 2-fold axis differ in length by a significant amount. The short Fe(1)–Fe(1)′ distances [2.733 (3) and 2.766 (3) Å, respectively for I and II] are found between the Fe atoms that are coordinated to the monodentate PhS^- and Cl^- ligands. These distances are virtually identical with the corresponding distances found in $Fe_4S_4(SPh)_2Cl_2^{2-}$ (Table VII) and other $[Fe_4S_4L_4]^{2-}$ cubanes. The "long" Fe(2)–Fe(2)′ distances account for the significant deviations from 60° of the Fe(2)–Fe(1)–Fe(2)′, Fe(1)′–Fe(2)–Fe(2)′; and Fe(1)–Fe(2)–Fe(2)′ angles at 66.63 (6)° and 65.44 (1)°, 56.66 (6)° and 56.36 (6)°, and 56.71 (5)° and 58.20 (6)° for I and II, respectively. These angular distortions underscore the deviations of the Fe_4 polyhedron from tetrahedral geometry toward a "butterfly" geometry. The

(22) Ileperuma, O. A.; Feltham, R. D. *Inorg. Chem.* **1975**, *14*, 3042.
(23) Coucouvanis, D. *Prog. Inorg. Chem.* **1979**, *26*, 301.
(24) If the midpoint of the Et_2Dtc sulfur atoms is considered as one coordination site, the distorted tetrahedral coordination around Fe(2) will be characterized by tetrahedral angles that range from 105.9 (3)° to 123.5 (4)°.
(25) Berg, J. M.; Holm, R. H. In "Iron-Sulfur Proteins"; Spiro, T., Ed.; Wiley-Interscience: New York, 1983; Vol. IV, p 27.

Table VII. Selected Structural Parameters of $Fe_4S_4(L)_x(Et_2Dtc)_{4-x}^{2-}$ (L = SPh, Cl, for x = 2 and L = Cl for x = 3), $Fe_4S_4(SPh)_2Cl_2^{2-}$, and $Fe_4S_4(S_2C_2(CF_3)_2)_4^{2-}$ Clusters

distances	$Fe_4S_4(SPh)_2$-$(Et_2Dtc)_2^{2-}$	$Fe_4S_4Cl_2$-$(Et_2Dtc)_2^{2-}$	$Fe_4S_4Cl_3$-$(Et_2Dtc)^{2-}$ [a]	Fe_4S_4-$(SPh)_2Cl_2^{2-}$	Fe_4S_4-$(S_2C_2(CF_3)_2)_4^{2-}$ [a,c]
Fe(1)–Fe(1)′	2.733 (3)	2.766 (3)	2.762 (3)	2.751 (3)	3.225 (7)
Fe(2)–Fe(2)′	3.053 (3)	3.045 (4)	2.936 (2)	2.770 (3)	3.222 (7)
Fe(1)–Fe(2)	2.780 (2)	2.845 (2)	2.849 (2)	2.738 (2)	2.731 (7)
Fe(1)–Fe(2)′	2.779 (2)	2.787 (2)	2.854 (2)	2.721 (2)	2.713 (7)
Fe(1)–S(1)	2.217 (4)	2.247 (3)	2.253 (2)	2.282 (3)	2.155 (10)
Fe(2)–S(2)	2.254 (3)	2.292 (4)	2.282 (2)	2.297 (3)	2.153 (11)
Fe(1)–S(2)	2.297 (3)	2.301 (4)	2.296 (2))	2.262 (3)	2.246 (10)
Fe(1)–S(2)′	2.307 (3)	2.306 (4)	2.307 (2)	2.282 (3)	2.257 (10)
Fe(2)–S(1)	2.364 (4)	2.410 (4)	2.372 (2)	2.269 (3)	2.245 (10)
Fe(2)–S(1)′	2.309 (4)	2.288 (4)	2.395 (2)	2.277 (3)	2.246 (10)
Fe(1)–S(t),(Cl)	2.281 (4)	2.249 (4)	2.231 (2)	2.261 (3)	
Fe(2)–S(1DT)	2.552 (4)	2.578 (4)	2.478 (2)		2.173 (10) [b]
Fe(2)–S(2DT)	2.436 (4)	2.421 (4)	2.469 (2)		
Fe(2)–Fe(1)–Fe(2)′	66.63 (6)	65.44 (6)	62.98 (4)	60.98 (5)	75.1 (3)
Fe(1)–Fe(2)–Fe(1)′	58.89 (6)	58.82 (6)	57.94 (4)	60.52 (5)	75.2 (3)
Fe(2)–Fe(1)–Fe(1)′	60.53 (5)	59.54 (6)	60.94 (4)	59.44 (5)	54.2 (3)
Fe(2)′–Fe(1)–Fe(1)′	60.58 (5)	61.64 (5)	61.12 (4)	60.04 (5)	54.3 (3)
Fe(1)′–Fe(2)–Fe(2)′	56.66 (5)	56.36 (6)	57.21 (4)	59.21 (5)	54.4 (3)
Fe(1)–Fe(2)–Fe(2)′	56.71 (5)	58.20 (6)		59.81 (5)	54.5 (3)
S(2)′–Fe(2)′–S(1)	96.44 (17)	97.49 (0)	97.96 (10)	102.28 (18)	
S(2)–Fe(1)–S(2)	104.30 (17)	103.45 (2)	104.60 (10)	102.58 (16)	

[a] These distances represent corresponding bonds in the Fe_4S_4 fragments of these compounds. An imaginary axis was assumed passing through the center of the Fe_4S_4 core in such a direction so that it corresponds to the crystallographic 2-fold of I and II.

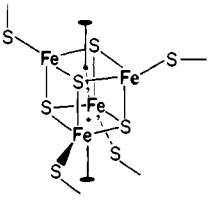

[b] Symmetric coordination. Average of eight values. [c] Reference 29.

four intermediate Fe(1)–Fe(2) distances in I and II have mean values of 2.780 (2) and 2.816 (2) Å, respectively. The Fe–S bonds can be divided into two sets of eight long (perpendicular to the 2-fold) and four short (parallel to the 2-fold) bonds. These differences reflect the compression of the Fe_4S_4 cores along the crystallographic 2-fold axes. The Fe–Fe–Fe angles divide into four sets (2 + 2 + 4 + 4). The above features are apparent in Table VII.

The possible C_{2v} symmetry in the Fe_4S_4 units of I and II is not realized because of significant asymmetry in the Fe(2)–S(1)–Fe(2)′–S(1)′ rhombic units. This asymmetry is more pronounced in II and is likely a result of the unequal Fe(2)–S(Et_2Dtc) bonds. Thus the longer Fe(2)–S(1) bonds [2.364 (4) Å in I and 2.410 (4) Å in II] are located trans to the long Fe(2)–S(1dt) bond, while the shorter Fe(2)–S(1)′ bonds [2.309 (4) Å in I and 2.288 (4) Å in II] are found trans to the short Fe(2)–S(2dt) bonds. This type of asymmetry is not observed in III, which contains almost equal Fe(2)–S(Et_2Dtc) bonds (vide infra).

Description of the Structure of $[Ph_4P]_2[Fe_4S_4Cl_3(Et_2Dtc)]$ (III)·DMF Complex. The structure of the anion in III is shown in Figure 3. Selected distances and angles of the anion in III are presented in Table VI. The crystal structure of III consists of well-separated cations and anions and DMF solvate molecules. The structures of the Ph_4P^+ cations and DMF molecules are unexceptional and will not be considered further.

The $[Fe_4S_4Cl_3(Et_2Dtc)]^{2-}$ anion is the first Fe_4S_4 cluster with a mixed ligand environment that contains different ligands in a ratio other than 1:1. Even though the anion does not have any crystallographically imposed symmetry, it does show approximate C_s symmetry (Figure 3) which is the highest idealized symmetry accessible. The plane of symmetry contains the atoms C(1dt), Fe(2), S(2), S(4), Fe(4), and Cl(4), none of which deviate from it by more than 0.016 Å.

In III as in I and II, two types of iron sites are found. The Fe(1), Fe(3), and Fe(4) sites are similar to the Fe(1) sites in I and II and the dimensions of the S_3FeCl tetrahedra are very close to the ones found in $[Fe_4S_4Cl_4]^{2-}$. The Fe–Cl distances range from 2.213 (2) to 2.249 (2) (Å) with a mean value of 2.231 (10) Å. The second iron site is bound to a Et_2Dtc ligand and involves five-coordinate Fe atoms. The geometry around the Fe(2) atom is that of a distorted square pyramid with atoms S(1)–S(3)–S(1dt)–S(2dt) defining a plane (maximum deviation from plane 0.04 Å) and constituting the "square" base of the pyramide. The equatorial S(2)–Fe(2)–S_{eq} angles range from 100.74 (1)° to 110.74 (10)° with a mean value of 105 (3)°. The Fe(2) atom is elevated from the basal plane by 0.60 (1) Å. The Fe(2)–S(2) vector in (III) deviates from the normal to the equatorial plane by 6°.

A closer look at the Fe_4S_4 core itself reveals that it is distorted with the Fe(2)–Fe(4) distance lengthened to 2.936 (2) Å (by comparison to the average 2.77 Å found in the conventional $[Fe_4S_4L_4]^{2-}$ cubanes). Two other distances that involve the Fe(2) atom, Fe(2)–Fe(1) and Fe(2)–Fe(3), have an "intermediate" value of 2.849 (2) and 2.854 (2) Å, respectively. The remaining Fe–Fe distances of atoms not involved with Et_2Dtc ligation show "normal" values ranging from 2.752 (2) to 2.771 (2) Å with a mean value of 2.762 (6) Å (Table VI).

The Fe–Fe distances in (III) divide into three sets (3 + 1 + 2), the Fe–S bonds into two sets (4 + 8), and the Fe–Fe–Fe angles into three sets (3 + 2 + 7). Since the Fe–S bonds divide metrically into four short bonds and eight long bonds, the Fe_4S_4 core can be regarded as compressed[26,27] along an axis that is perpendicular to Fe(1)–S(2)–Fe(3)–S(4) and Fe(2)–S(3)–Fe(4)–S(1) core faces. The "long" Fe(2)–Fe(4) distance accounts for the small but significant deviations of the Fe(2)–Fe(1)–Fe(4), Fe(2)–Fe(3)–Fe(4), and Fe(i)–Fe(2)–Fe(j) (i = 1, 3 and j = 3, 4) angles from 60°. These deviations are much more pronounced in I and II due to the corresponding longer Fe–Fe distance (vide supra). The ap-

(26) Mascharak, P. K.; Hagen, K. S.; Spence, J. T.; Holm, R. H. *Inorg. Chim. Acta* **1983**, *80*, 157.
(27) Lakowski, E. J.; Reynolds, J. G.; Frankel, R. B.; Foner, S.; Papaefthymiou, G. C.; Holm, R. H. *J. Am. Chem. Soc.* **1979**, *101*, 6562.

proximate C_s symmetry in III is realized because of the similarity of the Fe(2)–S(1) and Fe(2)–S(3) and Fe(4)–S(3) and Fe(4)–S(1) bonds, respectively (Table VI). Unlike I and II, the Et_2Dtc coordination to the Fe(2) atom is symmetric with roughly equal Fe(2)–S(Et_2Dtc) bonds [2.478 (2) and 2.469 (2) Å]. Like in I and II, the Fe(2)–S(1dt)–S(2dt)–C(1dt) portion of the anion is strictly planar.

Structure of the Fe_4S_4 Cores. In the structures of the mixed ligand cubanes $[Fe_4S_4(L)_2(L')_2]^{2-}$ with monodentate ligands such as $^-$SPh, $^-$OPh, and Cl^- the Fe_4S_4 core was found to possess approximate D_{2d} symmetry.[6] The placement of the Fe_4S_4 core in a mixed ligand environment in these cases did not cause any pronounced structural distortions other than slight deformations. The Fe_4S_4 unit had an overall noncompressed D_{2d} geometry and the Fe–Fe distances did not show any significant changes. This indicated that the monodentate ligands employed were electronically and sterically very similar to each other.

By contrast, the Fe_4S_4 cores in the $[Fe_4S_4(X)_n(Et_2Dtc)_{4-n}]^{2-}$ clusters show pronounced deviations from D_{2d} geometry with significant and systematic Fe–Fe and Fe–S distance changes. The Fe–Fe separations are the longest when the terminal ligands bound to the iron atoms are the chelating Et_2Dtc ligands and the associated bridging sulfide atoms are part of the square-pyramidal basal plane. It appears that Et_2Dtc ligand chelation and its orientation relative to the bridging sulfides determines the magnitude of the Fe–Fe distance elongation. This is clearly apparent in the structure of $[Fe_4S_4Cl_3(Et_2Dtc)]^{2-}$ where only one long Fe–Fe distance is observed.

An electronic origin for the large Fe–Fe separations in the $[Fe_4S_4]^{2+}$ core in I–III appears likely particularly when the unique electronic nature of the Et_2Dtc ligand is taken into account. A well-known[28] characteristic of the dithiocarbamate ligand is the ability to localize electron density on the sulfur donor atoms and to stabilize metal ions in high formal oxidation states. In R_2Dtc ligands with alkyl substituents, the contribution of the resonance form $R_2N^+{=}CS_2^{2+}$ is more pronounced. A donation of excess electron density from the R_2Dtc ligand to orbitals in the Fe_4S_4 unit, which are of slight antibonding character and have considerable Fe character, may result in an increase of the Fe–Fe distance. An increase in the Fe–Fe distances has been observed previously in the one-electron reduced Fe_4S_4 cores in the $[Fe_4S_4(SR)_4]^{3-}$ (R = Ph,[19] SCH_2Ph[20]) clusters.

Two other "cubane"-like Fe_4S_4 clusters that contain five-coordinate Fe atoms have been reported. The structure of $[Fe_4S_4(S_2C_2(CF_3)_2)_4]^{2-}$ was reported by Dahl et al.[29] and contains four five-coordinate iron sites with square-pyramidal geometry. The Fe_4S_4 core in this cluster is not isoelectronic to the cores in the clusters discussed herein.[30] However, this cluster also exhibits two long Fe–Fe bonds [3.225 (7) and 3.222 (7) Å] (Table VII) with a ligand orientation similar to that found in I–III. The Fe–Fe distance differentiation in this complex was explained in terms of electronic effects.[29] The second Fe_4S_4 cluster that contains a five-coordinate iron site was reported by Holm and co-workers.[31] In this case, the coordination around the iron atom is best described in terms of a trigonal-bipyramidal geometry rather than square pyramidal. The chelating ligand on the unique Fe atom is HOC_6H_4-*o*-S^- and the chelation results in two lengthened Fe–Fe distances of 2.839 (2) and 2.868 (2) Å, which are similar to the ones observed for the corresponding distances in III.

Finally, all $[Fe_4S_4]^{2+}$ cores in I–III contain Fe_2S_2 nonplanar rhombic faces and the diagonal Fe–S–Fe–S planes are nearly perfect. The Fe–Fe and Fe–S distances in the core fragments not associated with the Et_2Dtc ligand fall within ranges found in other isoelectronic Fe_4S_4 cores.[25]

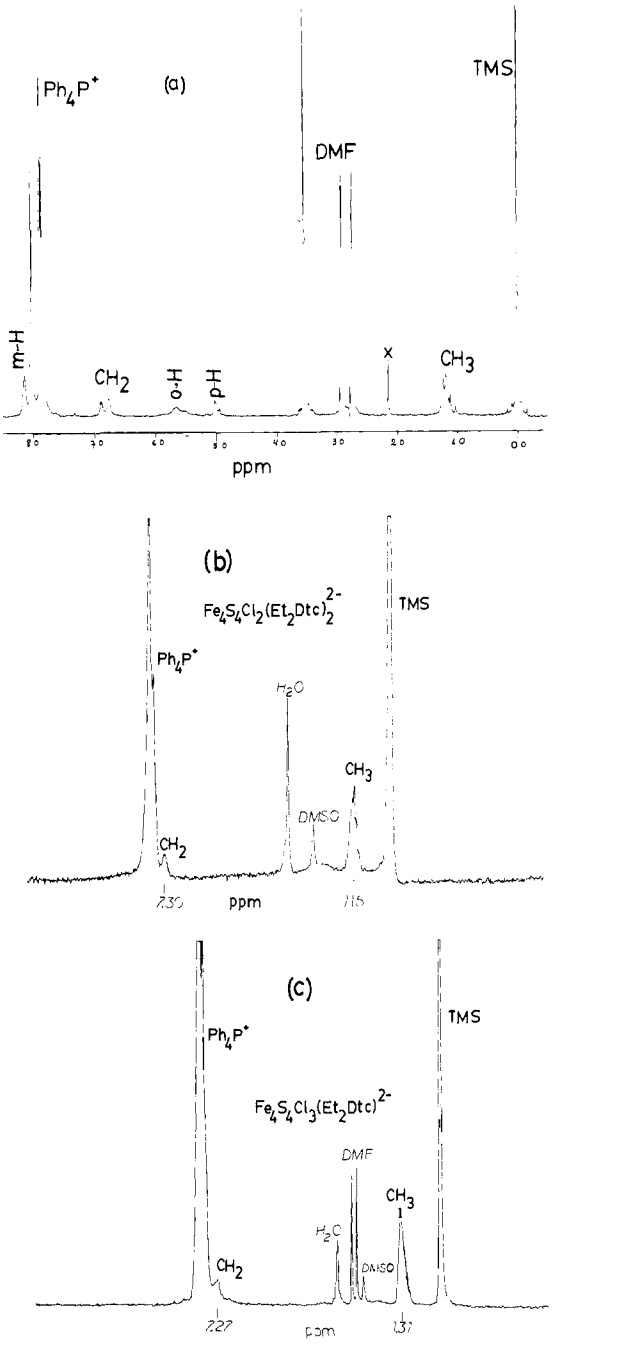

Figure 6. The FT ^1H NMR spectra at ambient temperature: (a) $[Fe_4S_4(SPh)_2(Et_2Dtc)_2]^{2-}$ (in DMF-d_7; 360 MHz); (b) $[Fe_4S_4Cl_2(Et_2Dtc)_2]^{2-}$ (in Me_2SO-d_6; 90 MHz); (c) $[Fe_4S_4Cl_3(Et_2Dtc)]^{2-}$ (in Me_2SO-d_6; 90 MHz).

3. ^1H NMR Spectroscopic and Solution Magnetic Studies. The $[Fe_4S_4(X)_n(Et_2Dtc)_{4-n}]^{2-}$ anions exhibit residual paramagnetism at room temperature. The magnetic moments of II and III (μ_{eff}^{corr}) were measured at 26 °C by the Evans NMR method[32] and were found to be 3.19 and 2.88 μ_B (per cluster), respectively. These values compare favorably with the ones found in the symmetric $[Fe_4S_4L_4]^{2-}$ clusters[33,34] and the mixed ligand $[Fe_4S_4(XPh)_2(L)_2]^{2-}$ (X = O, S; L = Cl, OPh) clusters[6] which range from 2.17 to 2.80 μ_B. The $[Fe_4S_4L_4]^{2-}$ complexes (L = $PhCH_2S^-$, PhS^-, Cl^-) in general exhibit antiferromagnetic behavior and are believed to possess diamagnetic (S = 0) ground states.[33] This conclusion has

(28) Coucouvanis, D. *Prog. Inorg. Chem.* **1970**, *11*, 233.
(29) Lemmen, T. H.; Kocal, J. A.; Yip-Kwai Lo, F.; Chen, M. W.; Dahl, L. F. *J. Am. Chem. Soc.* **1981**, *103*, 1932.
(30) The $[Fe_4S_4(L)_4]^{2-}$ and $[Fe_4S_4(X)_n(Et\ Dtc)_{4-n}]^{2-}$ clusters are thought to be isoelectronic. In ref 29, arguments are presented for the nonequivalency of the $[Fe_4S_4(L)_4]^{2-}$ and $[Fe_4S_4(S_2C_2(CF_3)_2)_4]^{2-}$ clusters. The latter formally contains the $[Fe_4S_4]^{6+}$ core, assuming the ligands to be dianions.
(31) Johnson, R. E.; Papaefthymiou, G. C.; Frankel, R. B.; Holm, R. H. *J. Am. Chem. Soc.* **1983**, *105*, 7280.
(32) Evans, D. F. *J. Chem. Soc.* **1959**, 2003.
(33) Papaefthymiou, G. C.; Laskowski, E. J.; Frota-Pessoa, S.; Frankel, R. B.; Holm, R. H. *Inorg. Chem.* **1982**, *21*, 1723.
(34) Frankel, R. B.; Averill, B. A.; Holm, R. H. *J. Phys.* (*Paris*) **1974**, *35*, C6-107.

Table VIII. Proton Isotropic Shifts[a] for the Et_2Dtc^- Ligand in $Fe_4S_4(X)_n(Et_2Dtc)_{4-n}^{2-}$ Complexes[b]

compound	CH_2 (ppm)	CH_3 (ppm)	ortho	meta	para
$[Ph_4P]_2Fe_4S_4(SPh)_2(Et_2Dtc)_2$[c]	−2.77	−0.08	1.44	−1.05	2.09
	−2.89	−0.13	1.60		2.16
$[Ph_4P]_2Fe_4S_4Cl_2(Et_2Dtc)_2$	−3.31	−0.05			
$[Ph_4P]_2Fe_4S_4Cl_3(Et_2Dtc)$	−3.28	−0.21			

[a] $(\Delta H/H_0)_{iso} = (\Delta H/H_0)_{diam} - (\Delta H/H_0)_{obsd}$. [b] In Me_2SO-d_6 solution. [c] Multiple signals due to the presence of at least one additional $[Fe_4S_4(SPh)_n(Et_2Dtc)_{4-n}]^{2-}$ congener.

been reached on the basis of variable-temperature (300 to 1.5 K) magnetic studies by Holm, Frankel, and co-workers.[33] As a result of the residual high-temperature paramagnetism, I–III exhibit isotropically shifted ^1H NMR spectra. The spectra of I (Figure 6a) show at least two resonances each for the Et_2Dtc protons and for the *o*-, *p*-, and *m*-phenyl protons and suggest that I may in fact contain significant amounts of mixed ligand clusters of the form $[Fe_4S_4(SPh)_2(Et_2Dtc)_{4-n}]^{2-}$.

The isotropic shifts of the ortho, meta, and para protons of the PhS^- ligands in I [and congener $[Fe_4S_4(SPh)_n(Et_2Dtc)_{4-n}]^{2-}$ clusters] occur according to the usual pattern of alternating signs and in CH_3CN-d_3 solution the resonances are centered around 5.72, 8.18, and 5.09 ppm, respectively. The origin of this pattern of isotropically shifted resonances in the $[Fe_4S_4(SPh)_4]^{2-}$ cluster has been attributed[35] to a dominant Fermi contact interaction propagated via a π-delocalization mechanism. A similar mechanism prevails in the $[Fe_4S_4(SPh)_n(Et_2Dtc)_{4-n}]^{2-}$ clusters although the inherent anisotropy in these molecules in principle could allow for a small dipolar contribution to the shifts as well. Typical NMR spectra of "I", II, and III are shown in Figure 6. The resonances for the CH_2 and CH_3 protons of the Et_2Dtc^- ligands in Me_2SO-d_6 are observed as broad signals at 6.94 and 1.19 ppm for I, 7.30 and 1.15 ppm for II, and 7.27 and 1.30 ppm for III, respectively. The corresponding signals in the diamagnetic Et_2Dtc^- free ligand ($Et_2DtcNa{\cdot}3H_2O$) are observed at 3.99 and 1.10 ppm, respectively. It is apparent that the isotropic shifts in all compounds decrease dramatically with distance from the paramagnetic center. In addition the isotropic shifts have the same signs (Table VIII). This behavior suggest that the shifts are due primarily to contact interactions with the spin transfer taking place through a direct σ-delocalization mechanism,[36] although a small dipolar (pseudocontact) contribution cannot be ruled out. The problem of dipolar contributions through space can only be satisfactorily settled by determination of molecular magnetic anisotropies. Estimates of the latter, however, are extremely difficult in these cases due to substantial thermal population of unknown magnetic states with unknown anisotropies. Similar phenomena have been observed previously in the proton NMR spectra of $FeX(Et_2Dtc)_2$ (X = Cl, Br, I) paramagnetic species.[37] They were interpreted in terms of dominant contact interactions through σ-bonds and virtually no dipolar contribution through space. Partial spin transfer through π-bonds within the pseudo aromatic

fragment, however, is still possible.

4. Electrochemical Studies. Previously,[6] the electrochemical behavior of $[Fe_4S_4(L)_2(L')_2]^{2-}$ complexes was described and was found to be similar to that of $[Fe_4S_4(L)_4]^{2-}$ with simple one-electron reversible reductions and irreversible multielectron oxidations. The electrochemical behavior of the $[Fe_4S_4(X)_n(Et_2Dtc)_{4-n}]^{2-}$ clusters is more complex than that of the mixed terminal ligand $[Fe_4S_4(L)_2(L')_2]^{2-}$ clusters reported[6] previously.

Table IX. Cyclic Voltammetric Results from $[Fe_4S_4(X)_n(Et_2Dtc)_{4-n}]^{2-}$ (X = SPh, Cl for n = 2 and X = Cl for n = 3)[a]

compound	E_{pc}	E_{pa}	ΔE, mV	i_{pa}/i_{pc}
	Reduction			
$[Fe_4S_4(SPh)_2(Et_2Dtc)_2]^{2-}$	−1.28			0.0
	−1.12	−1.01	111	0.45
$[Fe_4S_4(Cl)_2(Et_2Dtc)_2]^{2-}$	−1.24			0.0
	−1.16			0.0
$[Fe_4S_4(Cl)_3(Et_2Dtc)]^{2-}$	−1.10	−1.00	100	<0.2
	−0.90	−0.81	99	<0.3

	oxidation			
compound	E_{pa}	E_{pc}	ΔE, mV	i_{pc}/i_{pa}
$[Fe_4S_4(SPh)_2(Et_2Dtc)_2]^{2-}$	−0.250, −0.07[b]	−0.320	70	0.60
$[Fe_4S_4(Cl)_2(Et_2Dtc)_2]^{2-}$	−0.154	−0.257	103	0.55
$[Fe_4S_4(Cl)_3(Et_2Dtc)]^{2-}$	−0.130	−0.218	88	0.72

[a] Scan rate: 200 mV/s. [b] Ill-defined wave.

Table X. Double-Potential Step Chronamperometric Data for the Reduction and Oxidation of the $[Ph_4P]_2Fe_4S_4(SPh)_2(Et_2Dtc)_2$ on a Pt Bead Electrode at Ambient Temperature

reduction				
τ, s	i_c, μA	i_a, μA	$i_C\tau^{1/2}/C$, $(\mu A\ s^{1/2})/mM$	i_a/i_c
0.020	54.0	6.0	11.8	0.11
0.050	35.0	3.0	12.0	0.086
0.100	25.5	2.0	12.4	0.078
0.20	17.0	1.5	11.7	0.088
0.50	12.0	0.75	13.1	0.062
oxidation				
τ, s	i_a, μA	i_c, μA	$i_a\tau^{1/2}/C$, $(A\ s^{1/2})/mM$	i_c/i_a
0.020	58.0	19.0	12.6	0.33
0.050	34.5	9.5	11.9	0.29
0.10	24.8	6.75	12.1	0.27
0.20	19.2	4.0	13.2	0.21
0.50	13.2	2.5	14.4	0.19
1.0	10.5	1.7	16.2	0.16

[a] 0.65 mM $(Ph_4P)_2Fe_4S_4(SPh)_2(Et_2Dtc)_2$, 0.10 M, Pt electrode in DMF. [b] V vs. SCE. [c] $i_{pc}/v^{1/2}C$, $\mu A/[(V/s)^{1/2}\ mM]$.

The cyclic voltammetry of I (Table IX) shows both reduction and oxidation processes in the 0.0 to −1.4 V range. Two reduction waves are observed in DMF at −1.12 and −1.28 V. The former appears as a shoulder on the latter and carries appreciably less current. The oxidation occurs at −0.25 V and close to it another oxidation occurs at −0.07 V. Quantitative studies of these waves by cyclic voltammetry and chronoamperometry show that the redox processes are diffusion controlled over the range of 20 ms. Complete data are shown in Tables IX and X. The chronoamperometric current functions $i_ct^{1/2}/C$ and $i_at^{1/2}/C$ for the two reductions and the two oxidations combined correspond to one-electron processes. The reduction wave shows no associated anodic wave and therefore the process is irreversible. The oxidation wave at −0.25 V is accompanied by a small cathodic wave while the one at −0.07 V does not have a cathodic counterpart. The i_c/i_a and i_{pc}/i_{pa} ratios in chronoamperometry and cyclic voltammetry, respectively, show the oxidation product to be unstable. Chronoamperometry indicates that the oxidation product should be stable for about 100 ms. This is in agreement with the cyclic voltammetry results that show i_{pc}/i_{pa} ratios to increase with increasing scan rates.

The nature of the final oxidation product(s) currently is not known. However, similar oxidations of the $[Fe_4S_4X_4]^{2-}$ series of clusters (X = Cl^-, Br^-, I^-) have been reported recently to afford the new $[Fe_6S_6X_6]^{2-}$ clusters.[38]

(35) Holm, R. H.; Phillips, W. D.; Averill, B. A.; Meyerle, J. J.; Herskovitz, T. *J. Am. Chem. Soc.* **1974**, *96*, 2789.
(36) Horrocks, W. D., Jr. In "NMR of paramagnetic Molecules: Principles and Applications"; La Mar, G. N., Horrocks, W. D., Holm, R. H., Eds.; Academic Press: New York, 1973; Chapter 4.
(37) Dhingra, M. M.f Ganguli, P.; Mitra, S. *Chem. Phys. Lett.* **1974**, *25*, 579.
(38) Coucouvanis, D.; Kanatzidis, M. G.; Dunham, W. R.; Hagen, W. R. *J. Am. Chem. Soc.* **1984**, *106*, 7998.

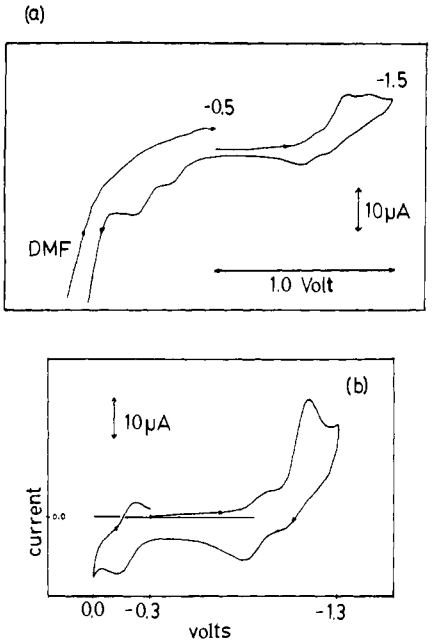

Figure 7. Cyclic voltammetric traces for (A) "$[Fe_4S_4(SPh)_2(Et_2Dtc)_2]^{2-}$" and (B) $[Fe_4S_4Cl_3(Et_2Dtc)]^{2-}$ in DMF solution. Scan rate: 200 mV s^{-1}.

Compounds II and III show similarly complicated electrochemical behavior. Two closely spaced cathodic irreversible waves and one anodic quasi-reversible wave corresponding to an oxidation process are observed for III. It is clear (Table IX) that the oxidation is irreversible in the chemical sense. All compounds show intense anodic waves at potentials greater than +0.4 V.

The apparent complexity of the redox properties of these compounds (Figure 7) and the fact that quantitatively the individual waves display current functions that correspond to less than one electron[39] imply that complex equilibria might be dominant features in solution. These equilibria could involve formation of statistical mixtures of mixed ligand species and/or dissociation of the Et_2Dtc^- ligands. The dynamic processes should be sufficiently slow relative to the cyclic voltammetric time scale and possibly could include reversible cluster transformations.

The $[Fe_4S_4L_4]^{2-}$ clusters generally undergo reversible one-electron reductions. The apparently different redox properties of I, II, and III must be attributed mainly to the Et_2Dtc ligand. The latter is known to stabilize high oxidation states in simple $M(Et_2Dtc)_n$ complexes.[23,28] The Et_2Dtc^- ligand appreciably influences the oxidation potential (Table IX) of a particular species in the order $[Fe_4S_4Cl_4]^{2-} < [Fe_4S_4(Cl)_3(Et_2Dtc)]^{2-} < [Fe_4S_4(Cl)_2(Et_2Dtc)_2]^{2-} < [Fe_4S_4(SPh)_2(Et_2Dtc)_2]^{2-} < [Fe_4S_4(Et_2Dtc)_4]^{2-}$. The last entry in the series exhibits a reversible 2−/1− couple.[18]

Mössbauer Spectra. As reported previously,[6] the $[Fe_4S_4L_2L_2']^{2-}$ clusters (L, L′ = Cl^-, PhS^-, PhO^-) with "mixed" *monodentate* terminal ligand environments do not show clearly discernible multiple iron sites in the Mössbauer spectra. These complexes display "simple", broad quadrupole doublets, and the widths of the resonance absorptions indicate that charge delocalization throughout the Fe_4S_4 core is extensive. To this extent they are not much different than the $[Fe_4S_4(L)_4]^{2-}$, identical terminal ligand clusters.

In the ^{57}Fe Mössbauer spectra of I–III, however (Table XI, Figure 8) site differentiation is apparent. The spectra consist of two superimposed distinct quadrupole doublets which can be assigned to the chemically and stereochemically different Fe sites (Figure 8).

A problem has been encountered in the Mössbauer spectra of the $[Fe_4S_4(SPh)_2(Et_2Dtc)_2]^{2-}$ cluster. The ratio of the two doublets in the spectra varies for different preparation of the compound

(39) According to the $i/(v^{1/2})\cdot C$, current function value.

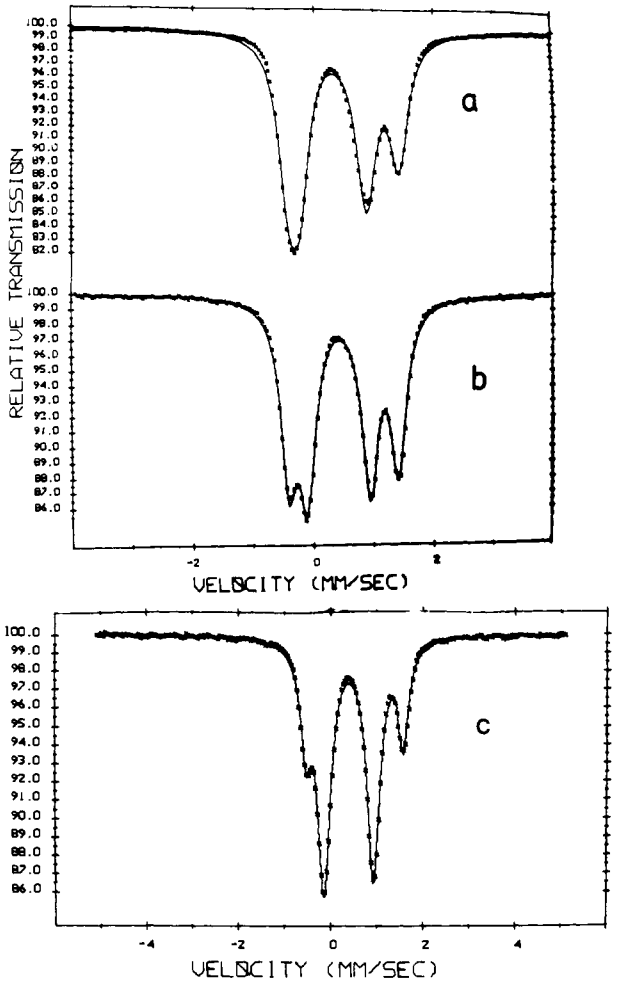

Figure 8. Mössbauer spectra at 77 K of (a) $[Fe_4S_4(SPh)_2(Et_2Dtc)_2]^{2-}$, (b) $[Fe_4S_4Cl_2(Et_2Dtc)_2]^{2-}$, and (c) $[Fe_4S_4Cl_3(Et_2Dtc)]^{2-}$. The solid lines are simulated spectra calculated with the parameters given in Table XI.

and for three different samples, a S_3FeEt_2Dtc to S_3FeSPh ratio of 1.60 ± 0.15 was found (77 K). This value is significantly different than the theoretically expected ratio of 1.00. Since the hyperfine parameters do not change from preparation to preparation, the variation in the sites ratio for this complex could be due to sample inhomogeneity. A mixture of $[Fe_4S_4(SPh)_x(Et_2Dtc)_{4-x}]^{2-}$ anions may be present in solution due to the possible equilibria:

$$2[Fe_4S_4(SPh)_2(Et_2Dtc)_2]^{2-} \rightleftarrows [Fe_4S_4(SPh)_4]^{2-} + [Fe_4S_4(Et_2Dtc)_4]^{2-}$$

and

$$2[Fe_4S_4(SPh)_2(Et_2Dtc)_2]^{2-} \rightleftarrows [Fe_4S_4(SPh)_3(Et_2Dtc)]^{2-} + [Fe_4S_4(SPh)(Et_2Dtc)_3]^{2-}$$

The coprecipitation of some or all of these species during the crystallization process would give rise to an inhomogeneous product. This explanation, which could account for the complex electrochemistry observed in solution (see above), is supported by the isotropically shifted ^1H NMR spectra. In the latter, the broad resonances (Figure 6) show structure that is indicative of a multicomponent system (Figure 6a).

The assignment of the sites assuming the "nested" configuration[40] was based on the unambiguously assigned spectrum of III (Figure 8). In the latter, the presence of two "nested" quadrupole doublets in a 3:1 ratio identified the unique Fe–Et_2Dtc site and the hyperfine Mössbauer parameters associated with it. An in-

(40) There are two ways of assigning the spectra: the "crossed" combination which is two interpenetrating quadrupole doublets and the "nested" combination where one quadrupole doublet is contained within the other.

Table XI. Isomer Shifts[a,b] and Quadrupole Splittings of $[Fe_4S_4(X)_n(Et_2Dtc)_{4-n}]^{2-}$ Complexes at 77 K (X = SPh, Cl)

	X site		Et_2Dtc site	
	IS_1, mm/s	ΔE_{Q1}, mm/s	IS_2, mm/s	ΔE_{Q2}, mm/s
$(Ph_4P)_2[Fe_4S_4(SPh)_2(Et_2Dtc)_2]$	0.47 (1)[c]	1.06 (1)[c]	0.64	1.84
$(Ph_4P)_2[Fe_4S_4(Cl)_2Et_2Dtc)_2]$	0.53	1.06	0.62	1.85
$(Ph_4P)_2[Fe_4S_4(Cl)_3(Et_2Dtc)]$	0.51	1.07	0.64	2.13
$(Et_4N)_2[Fe_4S_4(SC_6H_4\text{-}o\text{-}OH)_4]$[d]	0.42,[e] 0.46	0.76, 1.23	0.61	1.82
$(Ph_4P)_2[Fe_4S_4(SPh)_4]$	0.43	0.93		
$(Ph_4P)_2[Fe_4S_4(Cl)_4]$	0.49	0.67		
A. vinelandii FeMo protein P clusters[f]	0.69 (2) (Fe^{2+})	3.02 (2)	0.64 (2) (D)	0.81 (2)
C. pasteurianum FeMo protein P clusters[f]	0.64 (2) (Fe^{2+})	3.00 (2)	0.64 (2) (D)	0.70 (2)

[a] With respect to Fe metal at room temperature. [b] Results derived assuming the "nested" configuration. [c] Stimated uncertainty from the computer fitting. [d] From ref 31. [e] Literature data corrected to Fe metal at room temperature. [f] At 4.2 K. From ref 43.

dependent analysis of the spectra of I and II in the "nested" configuration[41] led to the hyperfine parameters similar to those predicted from the analysis applied for III (Table XI).

In this analysis, the tetrahedral, $LFeS_3$ sites show isomer shifts (IS) and quadrupole splittings (ΔE_Q) very similar to those found in the symmetric $[Fe_4S_4(L)_4]^{2-}$ clusters. A small but systematic increase appears, however, for the IS of these sites as the number of bidentate ligands increases in the molecule (~0.02 mm/s/Et_2Dtc, Table XI). This indicates a small increase of negative charge on these sites induced by the introduction of Et_2Dtc^- ligands on the remaining sites of the cubane. A pronounced increase in the IS values is found for the five-coordinated, Fe-Et_2Dtc sites. A similar increase has been reported[31] previously for the five-coordinate Fe site in the $[Fe_4S_4(SC_6H_4\text{-}o\text{-}OH)_4]^{2-}$ complex. The value of the IS observed for the five-coordinate Fe sites in these cubane structures lies between the values reported for the five-coordinate Fe(III) in $ClFe(Et_2Dtc)_2$[42] (0.49 mm/s, 100 K vs. Fe) and the five-coordinate Fe(II) in the $[Fe(Et_2Dtc)_2]_2$ dimer[43] (0.90 mm/s, 100 K vs. Fe). In the former case the Fe is coordinated in square-pyramidal geometry to four sulfurs on a plane and to one Cl^- on the apex while in the latter the apex is occupied by a S^- ligand. Taking into account an expected reduction of the IS value in replacing the Cl^- ligand by a S^- ligand in the Fe(III) complex we derive a mean value of ~0.65 mm/s for these two complexes which is indeed very close to the value observed for the five-coordinate Fe sites of the present complexes. We may conclude, therefore, that the observed increase of the IS value for these sites is primarily a result of a change in the coordination number from four to give and that these sites can also be assigned to a formal oxidation state of +2.5.

Summarizing, the Mössbauer results presented here for I–III and in the previous study[31] of the $[Fe_4S_4\text{-}(SC_6H_4\text{-}o\text{-}OH)_4]^{2-}$ cluster indicate that *changes in the IS values in clusters containing the Fe_4S_4 cores do not necessarily reflect changes in the overall oxidation state of the core.*

Conclusions. The introduction of bidentate terminal ligands on the $[Fe_4S_4]^{2+}$ cores results in significant core structural changes. These changes are not accompanied by dramatic charge localization. The substantial increases in the five-coordinate Fe–Et_2Dtc sites by ca. 0.16 mm/s must be attributed to the change in coordination number (and geometry) for these sites.

The P clusters of the FeMo proteins of nitrogenase exhibit a 3:1 distribution of sites D and Fe^{2+} in their spin-coupled diamagnetic state. The hyperfine parameters of the D components (Table XI) in *A. Vinelandii* and *C. pasteurianum* nitrogenases are similar to those for the five-coordinate sites in I–III. It appears that isomer shifts similar to those of the P clusters can be achieved without core reduction. It is also clear, however, that the complexes described here are not appropriate models for the P clusters for various reasons. Two of the complexes, I and II, do not have the desired 3:1 ratio. Complex III possesses different Fe sites with a 3:1 ratio but the five-coordinate site is the minor component. None of the compounds account for the apparent charge localization and the existence of the Fe^{2+} component in the P clusters. The Fe^{2+} component has been interpreted as a $Fe(II)S_4$ tetrahedral unit.[4,5] Finally, the complexes I–III do not exhibit reversible redox properties unlike the P clusters that show a one-electron oxidation to an EPR silent $S > {}^3/_2$ state.[4]

Acknowledgment. The financial support of this project by a Grant (No. GM26671-03) from the U.S. Public Health Service is gratefully acknowledged. We acknowledge Professors N. C. Baenziger of the University of Iowa and M. D. Ryan of Marquette University for fruitful discussions concerning the crystallographic and electrochemical aspects of this work, respectively.

Registry No. I, 83692-59-5; II, 88363-93-3; III, 97012-41-4; $[Ph_4P]_2Fe_4S_4(SPh)_2Cl_2$, 80939-30-6; $[Ph_4P]_2Fe_4S_4(SPh)_4$, 80765-13-5; $[Ph_4P]_2Fe_4S_4Cl_4$, 80765-12-4.

Supplementary Material Available: Listings of observed and calculated structure factors for compounds I–III and tables of positional and thermal parameters for all atoms in I, II, and III (62 pages). Ordering information is given on any current masthead page.

(41) In the original paper on the Mössbauer parameters for the $[Fe_4S_4\text{-}(SPh)_2(Et_2Dtc)_2]^{2-}$ cluster, IS, and ΔE_Q values of 0.74 and 1.67 and 0.39 and 1.34 mm/s were reported for the five-coordinate and the four-coordinate Fe sites, respectively.[7] These values were based on an assumed "crossed" combination for the two quadrupole doublets. At that time the $[Fe_4S_4Cl_3\text{-}(Et_2Dtc)]^{2-}$ cluster was not available.

(42) Chapps, G. E.; McCann, S. W.; Wickman, H. H. *J. Chem. Phys.* **1974**, *60*, 990.

(43) De Vries, J. L. K. F.; Keijzers, C. P.; De Boer, E. *Inorg. Chem.* **1972**, *11*, 1343.